

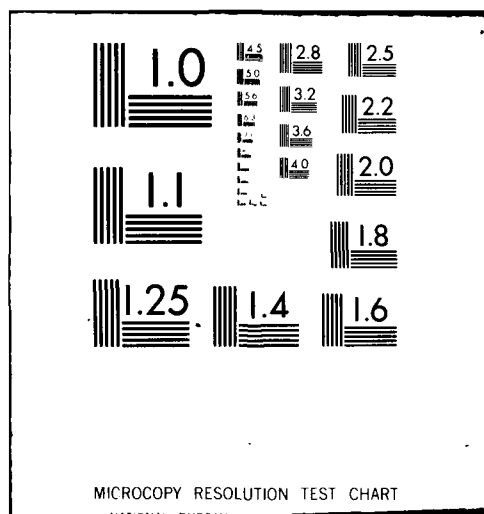
AD-A088 317

PROTOTYPE DEVELOPMENT ASSOCIATES INC SANTA ANA CA F/G 11/4  
AN ANALYSIS OF INTERLAMINAR STRESS GRADIENTS AND IMPACT DAMAGE --ETC(U)  
MAR 80 E L STANTON, L M CRAIN N62269-77-C-0144  
PDA-TR-5268-00-01 NADC-80135-60 NL

UNCLASSIFIED

1 of 1  
AD-A088 317

END  
DATE  
FILMED  
10-80  
DTIC



REPORT NO. NADC-80135-60

12771 12772

12  
6.5



# AN ANALYSIS OF INTERLAMINAR STRESS GRADIENTS AND IMPACT DAMAGE IN GRAPHITE-EPOXY LAMINATES

E. L. Stanton and L. M. Crain  
PROTOTYPE DEVELOPMENT ASSOCIATES, INC.  
1740 Garry Avenue  
Santa Ana, California 92705

March 1980

Final Report Under Contract No. N62269-77-C-0144

DTIC  
ELECTED  
AUG 27 1980

Approved for Public Release; Distribution Unlimited.

Prepared for  
NAVAL AIR DEVELOPMENT CENTER  
Warminster, Pennsylvania 18974

80 8 26 10

AD A088317

DDC FILE COPY

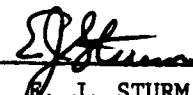
## NOTICES

**REPORT NUMBERING SYSTEM** - The numbering of technical project reports issued by the Naval Air Development Center is arranged for specific identification purposes. Each number consists of the Center acronym, the calendar year in which the number was assigned, the sequence number of the report within the specific calendar year, and the official 2-digit correspondence code of the Command Office or the Functional Directorate responsible for the report. For example: Report No. NADC-78015-20 indicates the fifteenth Center report for the year 1978, and prepared by the Systems Directorate. The numerical codes are as follows:

CODE	OFFICE OR DIRECTORATE
00	Commander, Naval Air Development Center
01	Technical Director, Naval Air Development Center
02	Comptroller
10	Directorate Command Projects
20	Systems Directorate
30	Sensors & Avionics Technology Directorate
40	Communication & Navigation Technology Directorate
50	Software Computer Directorate
60	Aircraft & Crew Systems Technology Directorate
70	Planning Assessment Resources
80	Engineering Support Group

**PRODUCT ENDORSEMENT** - The discussion or instructions concerning commercial products herein do not constitute an endorsement by the Government nor do they convey or imply the license or right to use such products.

APPROVED BY:

  
G. J. STURM  
CDR USN

DATE:

5/28/80

19 REPORT DOCUMENTATION PAGE		READ INSTRUCTIONS BEFORE COMPLETING FORM	
1. REPORT NUMBER NADC 80135-60	2. GOVT ACCESSION NO. AD-A088 317 (9)	3. RECIPIENT'S CATALOG NUMBER	
4. TITLE (and Subtitle) AN ANALYSIS OF INTERLAMINAR STRESS GRADIENTS AND IMPACT DAMAGE IN GRAPHITE-EPOXY LAMINATES		5. TYPE OF REPORT & PERIOD COVERED Final Report JAN 1977 to JAN 1978	
7. AUTHOR(s) E. L. Stanton and L. M. Crain		6. PERFORMING ORG. REPORT NUMBER PDA-TR-5268-00-01	
9. PERFORMING ORGANIZATION NAME AND ADDRESS Prototype Development Associates, Inc. 1740 Garry Avenue Santa Ana, CA 92705		8. CONTRACT OR GRANT NUMBER(s) N62269-77-C-0144	
11. CONTROLLING OFFICE NAME AND ADDRESS Aircraft and Crew Systems Technology Directorate Naval Air Development Center Warminster, PA 18974		10. PROGRAM ELEMENT, PROJECT, TASK AREA & WORK UNIT NUMBERS	
14. MONITORING AGENCY NAME & ADDRESS (if different from Controlling Office) 1286		12. REPORT DATE March 1980	
		13. NUMBER OF PAGES 77	
		15. SECURITY CLASS. (of this report) UNCLASSIFIED	
		15a. DECLASSIFICATION DOWNGRADING SCHEDULE	
16. DISTRIBUTION STATEMENT (of this Report)  Approved for public release; Distribution unlimited.			
17. DISTRIBUTION STATEMENT (of the abstract entered in Block 20, if different from Report)			
18. SUPPLEMENTARY NOTES			
19. KEY WORDS (Continue on reverse side if necessary and identify by block number) Composites                      Delamination Laminates                      Finite Element Interlaminar Stress Impact Damage			
20. ABSTRACT (Continue on reverse side if necessary and identify by block number) Interlaminar stress gradients caused by an internal disbond and by low velocity impact are analyzed using 3D finite elements. The disbanded [0/±45/0 <sub>2</sub> //45/45/0] laminate warps out-of-plane under biaxial compression without large stress gradients. A much thicker 48 ply laminate [±45/0 <sub>2</sub> /±45/0 <sub>2</sub> /±45/0/90] <sub>2s</sub> is analyzed for impact by a steel sphere that strikes the laminate off-center. Large sub-surface shear stresses occur around the perimeter of the contact area with a sinusoidal distribution. These results were obtained using the PATCHES-III program with new constraint elements for modeling laminates.			

## TABLE OF CONTENTS

<u>Section</u>	<u>Page</u>
1. INTRODUCTION AND SUMMARY	1
2. INTERLAMINAR STRESS FINITE ELEMENT MODELING	3
2.1 3D Composite Properties for Laminate Force- Deformation Behavior	3
2.2 Constraint Finite Elements	10
2.3 Interlaminar Modeling	11
3. DISBONDED LAMINATE ANALYSIS	17
3.1 Prototype Models	17
3.2 Laminate Finite Element Models	22
3.3 Disbonded Laminate Results	25
4. LAMINATE IMPACT ANALYSES	31
4.1 Thick Laminate Composite Response	31
4.2 Impact Site Model	34
4.3 Interlaminar Impact Stress Results	36
5. CONCLUSIONS AND RECOMMENDATIONS	43
6. REFERENCES	45
Appendix	A-1

Accession For	
1. Project	<input checked="" type="checkbox"/>
2. Report	<input type="checkbox"/>
3. Drawing	<input type="checkbox"/>
4. Photograph	<input type="checkbox"/>
5. Other	<input type="checkbox"/>
Date	
By	
Initial	
A	

## LIST OF FIGURES

<u>Figure</u>		<u>Page</u>
1.	PC Property Modeling Limits	7
2.	Interlaminar Normal Stress Comparisons	13
3.	PATCHES-III Transition Model for Interlaminar Stress Analysis	15
4.	Disbonded Laminate Schematic Using Diagonal Symmetry	15
5.	Two-Ply Disbond Prototype Model for Forces	20
6.	Interply Forces: [0/-45] Uniaxial Load	21
7.	Interply Forces: [0/45] Uniaxial Load	21
8.	Unbalanced Laminate Bending Displacements	23
9.	Normal Deformations in the Plies Adjacent to the Disbond	26
10.	Bottom Ply Shear Stress Changes	27
11.	Thick Laminate Impact Schedule	32
12.	Laminate Structural Response PATCHES-III Model	33
13.	Impact Site PATCHES-III Model	35
14.	Centerline Fiber Stress	37
15.	Cartesian Centerline Shear Strains	38
16.	Fiber Stresses Around Impact Perimeter	40
17.	Transverse Shear Stresses Around Impact Perimeter	40
18.	Ply Shear Stress Around Impact Perimeter	41
19.	Thick Laminate Local Bending Deformation Comparisons	42

## LIST OF TABLES

<u>Table</u>		<u>Page</u>
1.	Three-Ply Laminate Force-Deformation Properties	8
2.	Three-Ply Laminate Deformation-Force Properties	8
3.	Parametric Cubic Laminate Property Model	9
4.	Force-Deformation Comparisons	9
5.	PATCHES-III Finite Element Additions	10
6.	Interlaminar Normal Stress Comparisons	12
7.	Interlaminar Shear Stress Comparisons	14
8.	Graphite-Epoxy Nominal Elastic Properties	24
9.	Bonded Laminate Constraint Forces Through the Thickness at $r = 0$	24
10.	Disbonded Laminate Energy Change	25
11.	Disbonded Laminate Constraint Force Changes Through the Thickness at $r = 0$	27
12.	Disbonded Laminate Constraint Force Changes Through the Thickness at $r = R$	28
13.	Parametric Cubic Thick Laminate Property Model	34
14.	Thick Laminate Ply Stress Summary	41



## LIST OF SYMBOLS

<u>Letter</u>	<u>Definition</u>
$(A_n)_{ij}$	Integrated ply property moments; $n = 0,1,2$ .
$\bar{B}_{i\alpha}$	Composite stress-curvature stiffness constants from classical 3D lamination theory.
$\bar{C}_{ij}$	Composite stress-strain stiffness constants from classical 3D lamination theory.
$C_{ij}^*(\xi)$	Composite stress-strain parametric stiffness coefficients for 3D finite element laminate modeling.
CCL, etc.	Three character mnemonic defining 3D finite elements where C = cubic, L = linear indicate displacements in the coordinate directions associated with the character position.
$\bar{D}_{\alpha\beta}$	Composite moment-curvature stiffness constants from classical 3D lamination theory.
$\underline{e}_i$	Orthonormal Cartesian bases vectors.
$E_{ij}$	Orthotropic material extensional moduli.
$F_i(\xi)$	Parametric cubic Hermite functions.
$G_{ij}$	Orthotropic material shear moduli.
$P_{ijk}$	Tricubic Hermite coefficients in point format.
$R, r$	Radial coordinate.
$S_{ij}^*(\xi)$	Composite strain-stress parametric flexibility coefficients for 3D finite element laminate model.
$S_m$	Cubic Hermite coefficients in algebraic format.
$T_{mn}$	Point format cubic transformation matrix.
$Z_i$	Cartesian coordinate.
<u>Greek Letter</u>	<u>Definition</u>
$\delta_i$	Coefficients in the solution of the contact problem for transversely isotropic materials.
$\epsilon_i^*$	Composite strain component.
$\kappa_\alpha$	Laminate curvatures in the surface coordinate directions of the composite material.

Greek LetterDefinition $\nu_{ij}$ 

Orthotropic material Poisson ratios.

 $\sigma_i^*$ 

Composite stress component.

 $\xi_i$ Parametric coordinate  $0 \leq \xi_i \leq 1$ .

## 1. INTRODUCTION AND SUMMARY

The sensitivity of laminates to low velocity impact damage is a practical design problem that the ASTM and others have been investigating for several years. One of the difficulties in studying impact response is predicting the complex interlaminar stress gradients that it produces in composite structures. This report presents a systematic approach to interlaminar stress gradient modeling with applications to a graphite-epoxy laminate impacted by a steel sphere and a laminate with an internal disbond. The approach is based on a family of variable property finite elements for laminate models that transition to discrete ply models for regions with interlaminar stress gradients. All 45 elastic constants for a general anisotropic laminate are simulated and considerable error is shown to occur when uniform properties are used with certain laminate models. Careful modeling of the force-deformation behavior is required to predict accurate boundary conditions in the impact region when bending is present. Numerical results are presented for a thin 8 ply laminate and a thick 48 ply laminate.

The report first develops two new finite element modeling tools for interlaminar stress analysis and validates them using control problems with known solutions. The new analysis tools are composite property models that vary through the thickness to correctly model bending and linear element constraints for lamination theory force-deformation modeling. These tools are then used to analyze a thin laminate with an internal disbond and a thick laminate impacted at low velocity by a steel sphere. The disbond produces a locally unbalanced laminate that under biaxial compression warps badly with large out-of-plane displacements, but with very little internal force redistribution. These results were obtained from a model using two planes of symmetry that were found to introduce fictitious constraint forces between 0 and 45 degree plies at the laminate center. Results for the laminate impact problem were obtained from a complete 360 degree model of the impact site. A structural model of the entire laminate was used to obtain displacement boundary conditions for a discrete model of the impact site. These results show large subsurface shears at the perimeter of the contact area in the second ply below the surface. Only the top four plies were modeled individually to reduce costs, but more detailed models were prepared for later solution.

## 2. INTERLAMINAR STRESS FINITE ELEMENT MODELING

Recently finite element modeling approaches have been suggested for the determination of interlaminar stresses in those problems that cannot be solved using lamination theory [1,2,3]. All of these involve some form of ply-by-ply modeling and an appeal to St. Venants principle to allow a transition to composite laminate modeling away from the region of interlaminar stress gradients. The issues affecting the accuracy and efficiency of computational models for this class of problems are reviewed in this section and a systematic approach is presented for use with PATCHES-III. First a variable property simulation of laminate force-deformation behavior is introduced that can represent all 45 elastic constants necessary to characterize general anisotropic laminate deformations [4]. Next a family of linear constraint finite elements are developed from the PATCHES-III tricubic finite element to model the deformations of general laminates. The final and critical development for interlaminar stress gradient analysis is a procedure to transition from discrete 3D ply modeling to 2D+ composite laminate modeling. The features of this new system are then tested using the edge effect demonstration problem and a collection of balanced and unbalanced laminate problems.

### 2.1 3D COMPOSITE PROPERTIES FOR LAMINATE FORCE-DEFORMATION BEHAVIOR

Pagano [3] has shown that the forces and moments in a general anisotropic laminate are related to laminate strains and curvatures by 45 elastic constants in the equations

$$\left. \begin{aligned} \sigma_i^* &= \bar{C}_{ij} \epsilon_j^* + \bar{B}_{i\alpha} \kappa_\alpha \\ M_\beta/h^2 &= \bar{B}_{j\beta} \epsilon_j^* + \bar{D}_{\beta\alpha} \kappa_\alpha \end{aligned} \right\} \begin{array}{l} \text{for } 1 \leq i, j \leq 6 \\ \alpha, \beta = 1, 2, 4 \end{array} \quad (2.1)$$

which the PATCHES-III contracted convention is used with  $\epsilon_4$  defined as the in-plane shear strain. These equations reduce to the classical plate theory for laminates with monoclinic plies when  $\sigma_3 = 0$ . Once the volume average strains  $\epsilon_i^*$  and laminate curvatures  $\kappa_\alpha$  have been found, the individual ply stresses can be determined using ply properties  $C_{ij}$  and the relations developed by Pagano [4].

The elastic constants in Equation (2.1) are functions of the integrated moments of the ply properties

$$\left[ (A_0)_{ij}, (A_1)_{ij}, (A_2)_{ij} \right] = \int_{-h/2}^{h/2} \left[ 1, z_3, z_3^2 \right] c_{ij}(z_3) dz_3 \quad (2.2)$$

where the exact expressions for the  $\bar{C}_{ij}$ ,  $\bar{B}_{i\alpha}$ ,  $\bar{D}_{\alpha\beta}$  involve transformations arising from the assumption  $\sigma_3$ ,  $\sigma_5$ , and  $\sigma_6$  are each constant through the thickness. The approach developed in the present study uses these same moments to define a variable property composite material in the thickness direction with the same force-deformation behavior. When a finite element of this material is subject to the same volume average strains,  $\epsilon_i^*$ , and curvatures  $\kappa_\alpha$  as a laminate modeled using Equation (2.1), the same stress resultants will be produced. The converse of this will not be true in general unless displacement constraints are introduced in the thickness direction to prevent a pseudo edge effect from warping the cross-section. In this study, a linear displacement constraint in the thickness direction is used with the variable property model to define a CCL finite element that predicts the force-deformation behavior of Equation (2.1).

Consider a parametric cubic model for the property variation in the normal direction. This allows up to a sixth degree polynomial in  $Z_3$  when the thickness coordinate function,  $Z_3(\xi)$ , is also cubic. However, the use of nonuniform geometry models to aid in composite property modeling while feasible [Ref. 5] is not very convenient as it requires solving nonlinear equations. The use of a uniform (i.e., linear) geometry model for  $Z_3(\xi)$ ,

$$Z_3(\xi) = h(\xi - 1/2) \quad (2.3)$$

and a parametric cubic for each elastic constant in the thickness direction,

$$C_{ij}^*(\xi) = (S_m)_{ij} \xi^{4-m} \quad \text{for } 1 \leq m \leq 4 \quad (2.4)$$

is adequate for most laminates. In some extreme cases, it may be necessary to use nonuniform geometry modeling to avoid unreasonable values of  $C_{ij}^*(\xi)$  at local points through the thickness. However, it is always possible using

uniform models to match the integrated moments in Equation (2.2) which is the essential requirement for finite element modeling. Substituting this property model into Equation (2.2) results in four linear equations

$$(A_n)_{ij} = h^{n+1} \int_0^1 (\xi-1/2)^n \xi^{4-m} d\xi (S_m)_{ij}$$

for  $0 \leq n \leq 3$   
 $1 \leq m \leq 4$  (2.5)

These can be expressed in matrix form

$$A_n = T_{nm} S_m \quad (2.6)$$

for any component of  $C_{ij}(\xi)$  where

$$T_{nm} = \begin{bmatrix} h/4 & , & h/3 & , & h/2 & , & h \\ 3h^2/40 & , & h^2/12 & , & h^2/12 & , & 0 \\ 7h^3/240 & , & h^3/30 & , & h^3/24 & , & h^3/12 \\ 13h^4/1120 & , & h^4/80 & , & h^4/80 & , & 0 \end{bmatrix} \quad (2.7)$$

In the special case of a homogeneous laminate,  $A_1 = A_3 = 0$  with  $A_2 = A_0 h^2/12$ , the solution of Equation (2.6) results in simply  $C_{ij}^*(\xi) = (A_0)_{ij}/h$  as it must. It is possible to simulate  $A_0, A_1, A_2$  with only a quadratic, but the use of the full cubic reduces the number of pathological cases for which  $C_{ij}^*(\xi)$  may not be positive definite at all points through the thickness. It is important to note that this is strictly an interpolation problem that can be avoided at the expense of using more interpolation functions.

At this point, there are two issues to be resolved before the approach can be used. First, does the model accurately represent laminate force-deformation behavior, and secondly is there any significant difference with simple constant property models based on the rule of mixtures? The unbalanced laminate analyzed by Pagano [4] for uniaxial loading is used to answer both questions and to illustrate the practical limits of a uniform PC property model.

Consider the three-ply laminate [60/0/-60] with ply properties

$$\begin{aligned} C_{11} &= 210.35 \text{ GPa} & C_{22} &= C_{33} = 22.30 \text{ GPa} \\ C_{12} &= C_{13} = 7.01 \text{ GPa} & C_{23} &= 5.75 \text{ GPa} \\ C_{44} &= C_{55} = 10.34 \text{ GPa} & C_{66} &= 4.14 \text{ GPa} \end{aligned}$$

as taken from Pagano [2.4] where the msi units of that paper are retained for comparison. These ply properties result in the force-deformation properties shown in Table 1 and their inverse shown in Table 2. Under uniaxial load, for example, the laminate twists and stretches with the deformations given by the corresponding column in Table 2. Consider now the representation of this behavior using  $C_{ij}^*(\epsilon)$  determined from Equation (2.6). These property functions in PC point format are displayed in Table 3. Note that the extensional moduli were not determined from Equation (2.6), but are the same constants as in Table 1. The reason for this is evident in Figure 1 which shows the PC function for  $C_{11}^*(\epsilon)$ . The discrete ply  $C_{11}$  properties vary so sharply that their standard deviation, 14.59, is larger than their mean value, 13.66. To represent  $A_0$ ,  $A_1$ , and  $A_2$  in this case, a uniform PC function must overshoot zero near the upper and lower surfaces which if used would violate positive definite  $C_{ij}$  requirements at these points. To avoid this, only  $A_0$  and  $A_1$  were simulated by the property model in Table 3, and as a result the bending-curvature properties ( $M_1$ ,  $M_2$  loading) are not correct. All other force-deformation properties should be exact, and in particular the uniaxial case analyzed by Pagano,  $\sigma_1^* = 1$ , should be modeled correctly. This was tested using one CCL element in PATCHES-III with Table 3 material properties and loaded by a uniform pressure on opposite faces. The computed laminate strains,  $\epsilon_i^*$ , and curvatures  $\kappa_1$ ,  $\kappa_2$ ,  $\kappa_4$  were the same as the Pagano results, Table 4. The results from a unit moment,  $M_1 = 1.0$ , case are also compared in Table 4, and these deformations are much too low. The bending errors are a direct consequence of the bending stiffness error caused by using constant  $C_{11}$  and  $C_{22}$  properties from the rule-of-mixtures. In this laminate, [60/0/-60], the stiffness error is over 100 percent, and even in a balanced structural laminate, errors of 10 percent to 20 percent are common.

Consider as an example of this behavior the 48 ply laminate analyzed later in this report. The property distribution (c.f. page 34) shows variable

C14 and C24 coupling through the thickness. This is necessary to account for the bending-shearing coupling  $(A_2)_{14}$  and  $(A_2)_{24}$  in this laminate which is quite strong. Note that representing this behavior is important to correctly predict the 3D deformation response of the laminate in areas of high local bending.

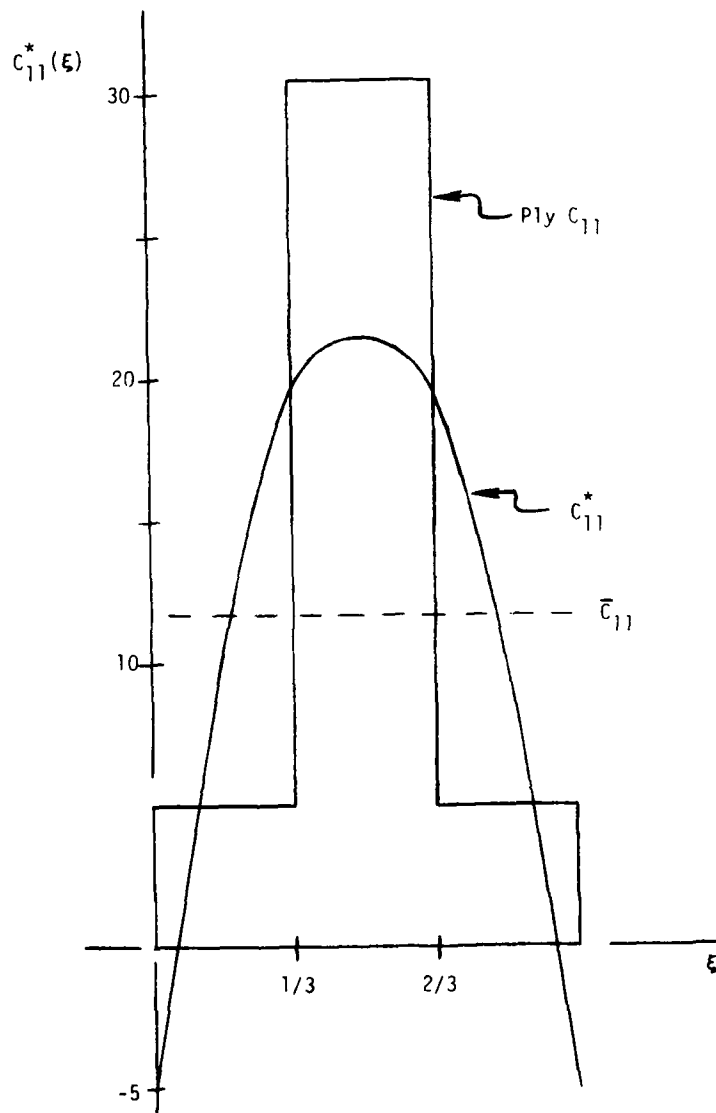


Figure 1. PC Property Modeling Limits



TABLE 1. THREE-PLY LAMINATE FORCE-DEFORMATION PROPERTIES  
( $10^6$  PSI)

	$\epsilon_1^*$	$\epsilon_2^*$	$\epsilon_3^*$	$\epsilon_4^*$	$\epsilon_5^*$	$\epsilon_6^*$	$\kappa_1^*$	$\kappa_2^*$	$\kappa_4^*$
$\sigma_1^*$	13.656	4.232	0.925						-0.694
$\sigma_2^*$		13.656	0.925						-1.930
$\sigma_3^*$			3.234						-0.018
$\sigma_4^*$				4.712			-0.689	-1.925	
$\sigma_5^*$					0.857				
$\sigma_6^*$		(SYM)				0.857			
$M_1^*$							0.494	0.450	
$M_2^*$								1.500	
$M_4^*$									0.512

TABLE 2. THREE-PLY LAMINATE DEFORMATION-FORCE PROPERTIES

	$\sigma_1^*$	$\sigma_2^*$	$\sigma_3^*$	$\sigma_4^*$	$\sigma_5^*$	$\sigma_6^*$	$M_1^*$	$M_2^*$	$M_4^*$
$\epsilon_1^*$	0.082	-.018	-.018						0.042
$\epsilon_2^*$		0.167	-.039						0.602
$\epsilon_3^*$			0.325						0.160
$\epsilon_4^*$				0.453			0.141	0.439	
$\epsilon_5^*$					1.167				
$\epsilon_6^*$		(SYM)				1.167			
$\kappa_1^*$							2.829	-.668	
$\kappa_2^*$								1.559	
$\kappa_4^*$									4.272

TABLE 3. PARAMETRIC CUBIC LAMINATE PROPERTY MODEL\*

	$C_{ij}^*(0)$	$C_{ij}^*(1/3)$	$C_{ij}^*(2/3)$	$C_{ij}^*(1)$
$C_{11}$	13.658	13.658	13.658	13.658
$C_{12}$	4.231	4.231	4.231	4.231
$C_{13}$	.926	.926	.926	.926
$C_{14}$	3.084	1.827	-1.827	-3.084
$C_{22}$	13.658	13.658	13.658	13.658
$C_{23}$	.926	.926	.926	.926
$C_{24}$	8.581	5.085	-5.085	-8.581
$C_{33}$	3.234	3.234	3.234	3.234
$C_{34}$	.078	.046	-.046	-.078
$C_{44}$	8.284	3.523	3.523	8.284
$C_{55}$	.550	1.217	1.217	.550
$C_{56}$	.385	.228	-.228	-.385
$C_{66}$	1.550	.833	.833	1.550

\*Only extensional force-deformation properties simulated.

TABLE 4. FORCE-DEFORMATION COMPARISONS

	$\epsilon_1^*$	$\epsilon_2^*$	$\epsilon_3^*$	$\epsilon_4^*$	$\kappa_1$	$\kappa_2$	$\kappa_4$
Exact ( $\sigma_1^* = 1$ )	.0823	-.0184	-.0184	.0	.0	.0	.0416
CCL ( $\sigma_1^* = 1$ )	.0822	-.0184	-.0180	.0	.0	.0	.0415
Exact ( $M_1^* = 1$ )	.0	.0	.0	.141	2.829	-.668	.0
CCL ( $M_1^* = 1$ )	.0	.0	.0	.065	.978	-.193	.0

\*Only extensional force-deformation properties simulated.

## 2.2 CONSTRAINT FINITE ELEMENTS

The CCL finite element used to model laminate force-deformation behavior is one of a family of linear constraint options developed for the PATCHES-III program. The need for low cost modeling in regions of uniaxial or biaxial strain was noted in an earlier report [6] and the new elements in Table 5 provide this capability. They are based on the linear constraints defined in Equation (2.8)

$$P_i = T_{i\alpha} P_\alpha \quad i = 1, 2, 3, 4$$

$$\alpha = 1, 4 \quad (2.8)$$

where the coefficients  $T_{i\alpha}$  are simply

$$T_i = \begin{bmatrix} 1 & , & 0 \\ 2/3 & , & 1/3 \\ 1/3 & , & 2/3 \\ 0 & , & 1 \end{bmatrix} \quad (2.9)$$

The same coefficients apply to all three parametric coordinates and, in general,

$$P_{ijk} = T_{i\alpha} T_{j\beta} T_{k\gamma} P_{\alpha\beta\gamma} \quad (2.10)$$

If constraints are introduced in only two coordinates,

$$P_{ijk} = T_{i\alpha} T_{j\beta} \delta_{kl} P_{\alpha\beta l} \quad (2.11)$$

and for only one constraint

$$P_{ijk} = T_{i\alpha} \delta_{jl} \delta_{km} P_{\alpha lm} \quad (2.12)$$

TABLE 5. PATCHES-III FINITE ELEMENT ADDITIONS

Displacements*	Nodes	Geometry	Properties
LLL	8	CCC	CCC
LLC	16	CCC	CCC
LCC	32	CCC	CCC
CCC	64	CCC	CCC

\*Any combination of L and C is available; L = Linear, C = Cubic.

Two key issues affecting the development of the new family of elements are how to efficiently generate their stiffness matrices and how to connect them to each other. After some early confusion, it was determined that all linear constraints can be applied before integration with the same result as when they are applied after integration. This greatly reduces the cost of generating their stiffness matrices. It is simple to demonstrate this equivalence in one dimension where obviously

$$\begin{aligned}
 K_{\alpha\beta}^P &= \int T_{i\alpha} F_i(\xi) F_j(\xi) T_{j\beta} d\xi \\
 &= T_{i\alpha} \int F_i(\xi) F_j(\xi) d\xi T_{j\beta} \\
 &= T_{i\alpha} K_{ij}^P T_{j\beta}
 \end{aligned} \tag{2.13}$$

but in higher dimensions interpolatory quadrature is used in PATCHES-III and this caused some concern at first.

The second issue was resolved by automating the generation of interface constraints between elements of different dimension. This allows the user of PATCHES-III to specify linear constraints on any element or group of elements by simply placing a mnemonic of the type listed in Table 5 on the connectivity card for that element. The program first generates all explicit mesh point constraints and then on a second pass generates all interface or implicit constraints. This requires extensive checking for conflicts, and in order to reduce their incidence, all three displacement components are constrained alike. At every constrained mesh point, one of the Equations (2.10)-(2.12) is automatically generated and applied to all affected matrices.

### 2.3 INTERLAMINAR MODELING

The use of substructuring to transition from discrete ply molding to composite laminate modeling was recently investigated by Wang and Crossman [2]. The same technique has been used for other composites under the name "minimechanics" [7] and, of course, it has been used for years in aircraft structural analysis. Substructuring in the case of laminates must account for two transition conditions: one along a plane defined by a ply, and the other along a plane normal to the laminate. The first case requires no transition in the shape of the finite element mesh and appears to work well for edge

effects caused by uniaxial loading [2]. Substructuring for the second case will require mesh changes, as well as the transition to composite properties. An approach using the new CCL finite element with laminate properties is evaluated in this section.

Consider the interlaminar stress problem analyzed in the PATCHES-III User's Manual. First, the accuracy of the new constraint finite elements will be demonstrated for the same four element model using the original properties. The two interior elements were constrained to be all linear (LLL) and the two edge elements were constrained linear in the direction of the load (LCC). No significant change in the earlier results should occur because the displacement solution has the same form in these regions. Normal stress comparisons in Table 6 show this to be true even though the model has been reduced to only 92 degrees-of-freedom. In fact, the assumption of linear displacements in the thickness direction (LCL) also was used with very little mid-surface normal stress error as comparisons in Figure 2 show. Interlaminar stress gradients between the  $0^\circ$  and  $90^\circ$  plies, however, are drastically changed in the LCL model as the shear stress comparisons in Table 7 show. Note that the interlaminar shear stress appears to contain a singularity at the free-edge between the  $0^\circ$  and  $90^\circ$  plies,  $\sigma_{23}(0,b,h)$ . The uniform mesh model gives the mean value of  $\sigma_{23}$ , but one element cannot model this response and return to zero at the free-edge. A nonuniform mesh element does a better job of matching this condition and produces about as much accuracy as can be expected from a single LCC element.

TABLE 6. INTERLAMINAR NORMAL STRESS COMPARISONS\*

$\xi/2h$ **	CCC/CCC (428 D.O.F.)	LLL/LCC (92 D.O.F.)	LLL/LCL (44 D.O.F.)
0	+2.95	+2.89	+2.76
1/3	- .26	- .27	- .31
2/3	- .43	- .44	- .25
1	- .16	- .05	- .03
2	- .02	- .03	- .03
3	+ .01	- .01	- .00
4	- .01	+ .02	- .02

\*Comparisons at midsurface between  $90^\circ$  plies.

\*\* $Z_2 = b - \xi$ ; distance from free-edge.

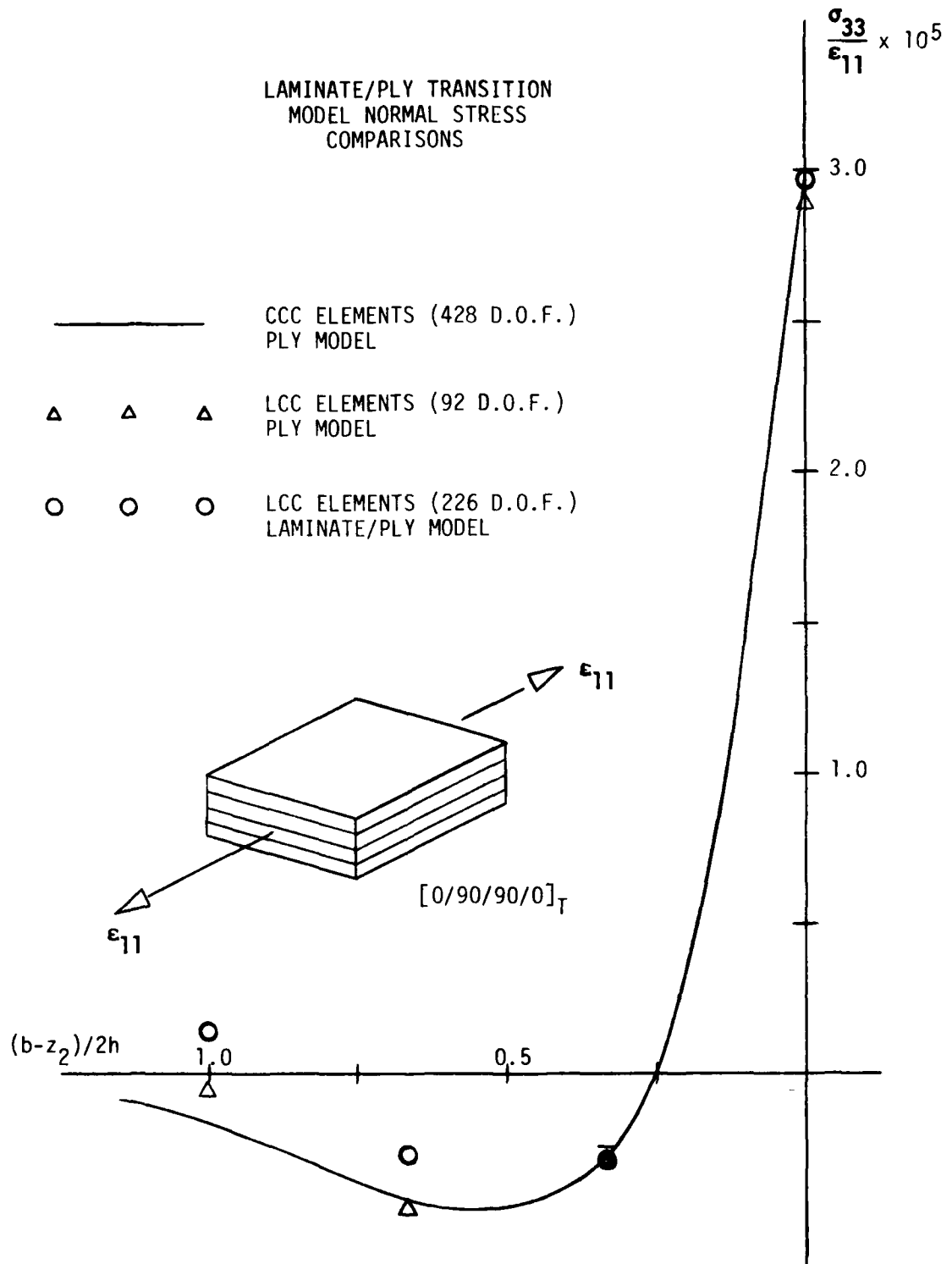


Figure 2. Interlaminar Normal Stress Comparisons

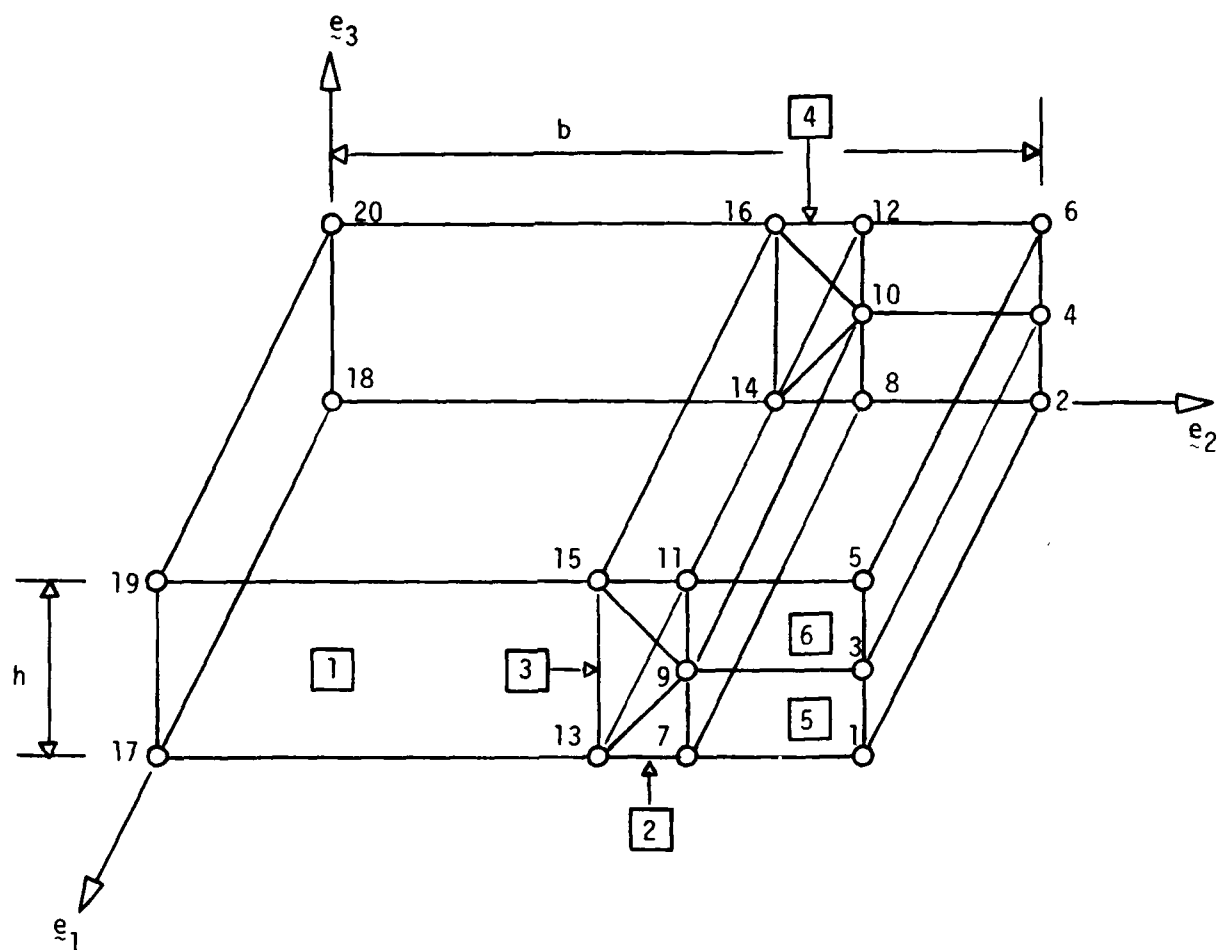
TABLE 7. INTERLAMINAR SHEAR STRESS COMPARISONS\*

$\xi/2h$	CCC/CCC Uniform	LLL/LCC Uniform	LLL/LCL Uniform	$\xi/2h$	LLL/LCC Nonuniform**
0	-2.72	-2.72	-.33	0	+ .58
1/3	- .85	- .85	-.47	1/9	-1.94
2/3	- .60	- .60	-.42	4/9	- .67
1	+ .03	+ .03	+.03	1	- .31
2	- .05	- .05	-.04	2	- .03
3	- .02	- .02	-.02	3	- .02
4	.00	.00	.00	4	.00

\*Comparisons between  $90^\circ$  and  $0^\circ$  plies.

\*\* $Z_2 = 6 + 4\xi - 2\xi^2$  (edge elements only).

Consider now the transition from discrete ply properties to a composite property model  $C_{ij}^*$  away from the free-edge. A six element model shown in Figure 3 was used to determine model accuracy when transitions of this type are made using the present constraint finite elements. Note the two edge elements are exactly as before, and the transition mesh uses three wedge shaped elements. Rule-of-mixture composite properties were used for elements number one and three, and all other elements use local ply properties as in the original model. The interlaminar stresses at the free edge changed very little, Figure 2. At the interface, of course, small local shear stresses occur because of the discrete change in properties. Their maximum value is less than one-half of one percent the applied axial stress. Essentially, the same results were obtained using  $C_{ij}^*(\xi)$  variable composite properties. Interestingly, the two ply laminate properties were easier to model with a cubic than the three ply laminate because the  $[0/90]$  properties are an odd function. These results indicate the transition from discrete ply modeling to composite laminate modeling can be made using the new constraint elements.



ELEMENT	DISPLACEMENTS	PROPERTIES
1	LCC	LAMINATE , LLC
2	LCC	PLY , 90°
3	LCC	LAMINATE , LLC
4	LCC	PLY , 0°
5	LCC	PLY , 90°
6	LCC	PLY , 0°

Figure 3. PATCHES-III Transition Model for Interlaminar Stress Analysis



### 3. DISBONDED LAMINATE ANALYSIS

The effects of an unsymmetric disbond on laminate deformations and associated internal load redistributions around the disbond are investigated for a thin laminate. An important aspect of the unsymmetrically disbanded laminate problem not considered in the present investigation is the effect of laminate thickness. There is considerable experimental evidence, Williams [8, 9], that the strength of thick laminates (~50 plies or more) is sensitive to internal disbonds in both unidirectional tape and bidirectional fabric materials of graphite-epoxy. These remarks refer to compressive not tensile loads and to disbonds between plies that occur without fiber damage. Results from the present investigation suggest thin laminates (~10 plies or less) will experience a loss in stiffness caused by out-of-plane bending before any stress critical failure. The laminate in this study is an eight ply graphite-epoxy flat panel with a small circular disbond ( $T/R \cong 0.1$ ) located three plies from the surface and at the center of the panel. A ply-by-ply modeling of this problem is used to study interlaminar force-deformation behavior in the vicinity of the disbond with CCL finite elements. No attempt was made to include in the model any strain singularities that might exist, although this could have been done had fracture mechanics been the focus of the study. The objective was to determine the deformations and internal load redistribution caused by an unsymmetric disbond in a compressively loaded thin laminate.

The disbanded laminate problem was analyzed early in the study using symmetry boundary conditions on two planes. Prototype models indicated a definite skewed displacement response would occur and that the use of symmetry planes would inhibit some response modes. Unfortunately, PATCHES-III was limited to 50 elements at that time and no practical means of avoiding symmetry modeling was available. The resulting symmetry model solution is essentially a 3D laminate solution with interlaminar stress gradients distorted at the origin by the symmetry boundary conditions. However, the force-deformation behavior of the laminate is represented reasonably well and several interesting conclusions can be drawn from the symmetry solution.

#### 3.1 PROTOTYPE MODELS

A schematic of the idealized disbanded laminate analyzed in this study is shown in Figure 4. The disbanded region is at the center of a square

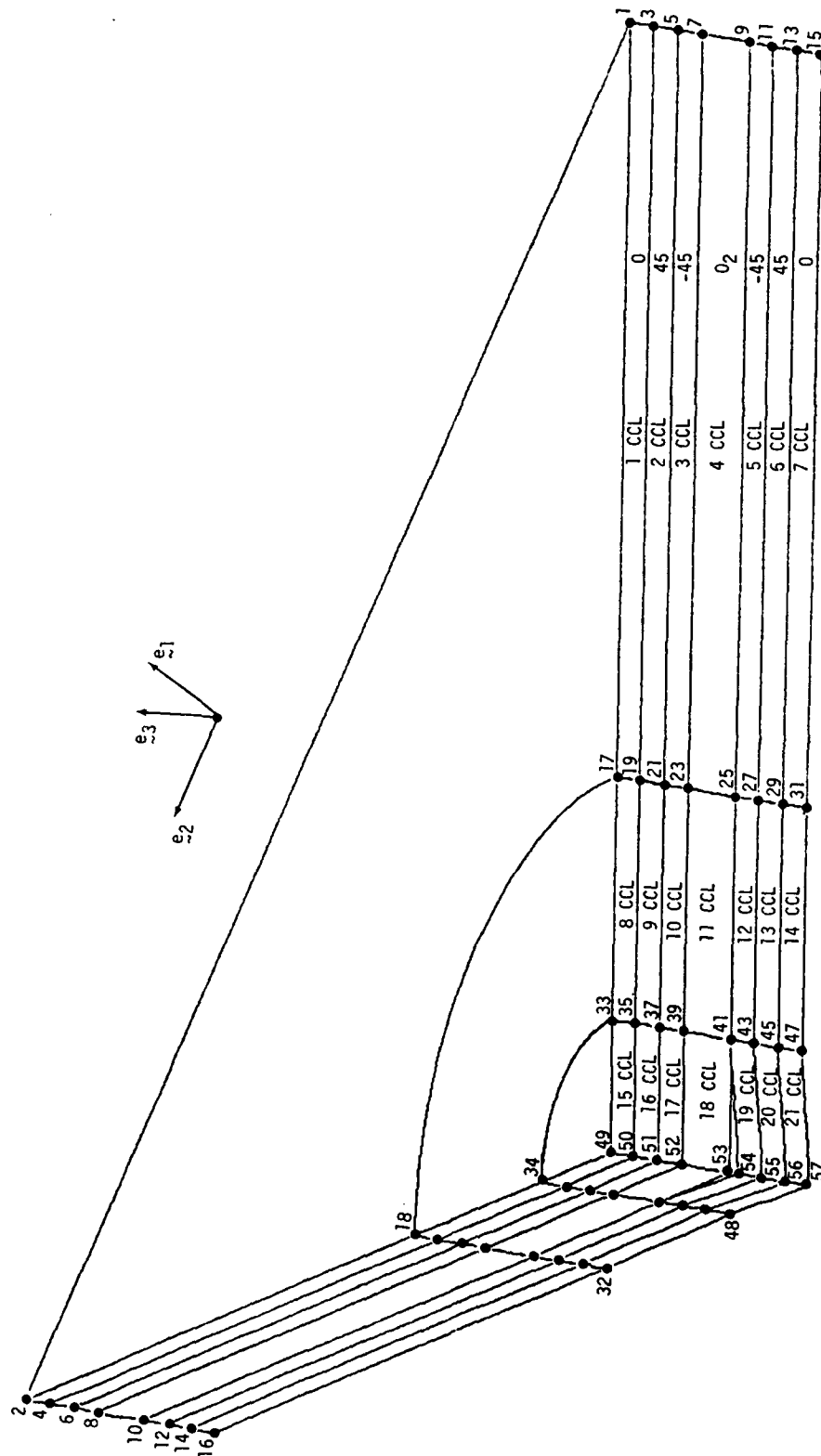


Figure 4. Disbonded Laminate Schematic Using Diagonal Symmetry

laminate between plies five ( $-45^0$ ) and six ( $0^0$ ). The region is circular with a bubble shape whose profile is given by

$$Z_3 = t_p(1 + \cos r\pi/R)/2 \quad (3.1)$$

where  $t_p$  is a ply thickness and the maximum radius is  $R = 1.27$  cm (0.5 in.). Note that this shape is tangent to the adjacent bonded region and corresponds to an elastically warped surface. A catenary shape would correspond to inelastic fiber damage at the boundary of the disbonded region. The laminate is 15.24 cm (6 in.) square and uniformly compressed 0.01524 cm (.006 in.) in both the  $e_1$  and  $e_2$  directions. At the loaded edges, the normal displacement component,  $u_3$ , is restrained to zero. The disbonded plies  $[-45/45/0]$  are unbalanced and after their separation, the remaining plies  $[0/45/-45/0_2]$  are also unbalanced. As in the unbalanced three-ply laminate analyzed by Pagano, there will be stretching-twisting coupling that must be considered in selecting a symmetry model. It is also important to examine the inplane force changes caused by a disbond to assist in preparation of the ply-by-ply model of the laminate.

A small two element model was used to examine interply force changes when a  $-45^0$  ply and a  $0^0$  ply disbond locally. The prototype model, Figure 5, consists of a  $-45^0$  ply and a  $0^0$  ply in one quadrant of the laminate (7.62 cm) loaded by a uniform strain  $\epsilon_{11} = 0.001$ . To simulate the disbond, the two elements were disconnected at node 8 corresponding to the center of the laminate. The two elements were type LLL and the nodal forces at the interply corners were used to measure the effect of the disbond. These are shown in Figure 6 and indicate only a small constraint force is relaxed by a disbond at node 8. Note, however, that the effect is to increase the transverse load in the  $0^0$  ply which carries most of the load associated with the applied  $\epsilon_{11}$  strain. It is obvious that a larger change will occur if either nodes 5 or 7 are cut instead of node 8 which is analogous to a disbond at node 8 in a  $+45/0^0$  layup. Results from this case, Figure 7, do show a larger change, but it reduces the transverse load in the  $0^0$  ply. The directional dependence in stiffness produces a directional dependence in the effect of a disbond under any given load. In this case of a circular disbond, Figure 4, under biaxial load, it appears that interply constraint forces will vary around the perimeter with relative maximums or minimums every  $45^0$ .

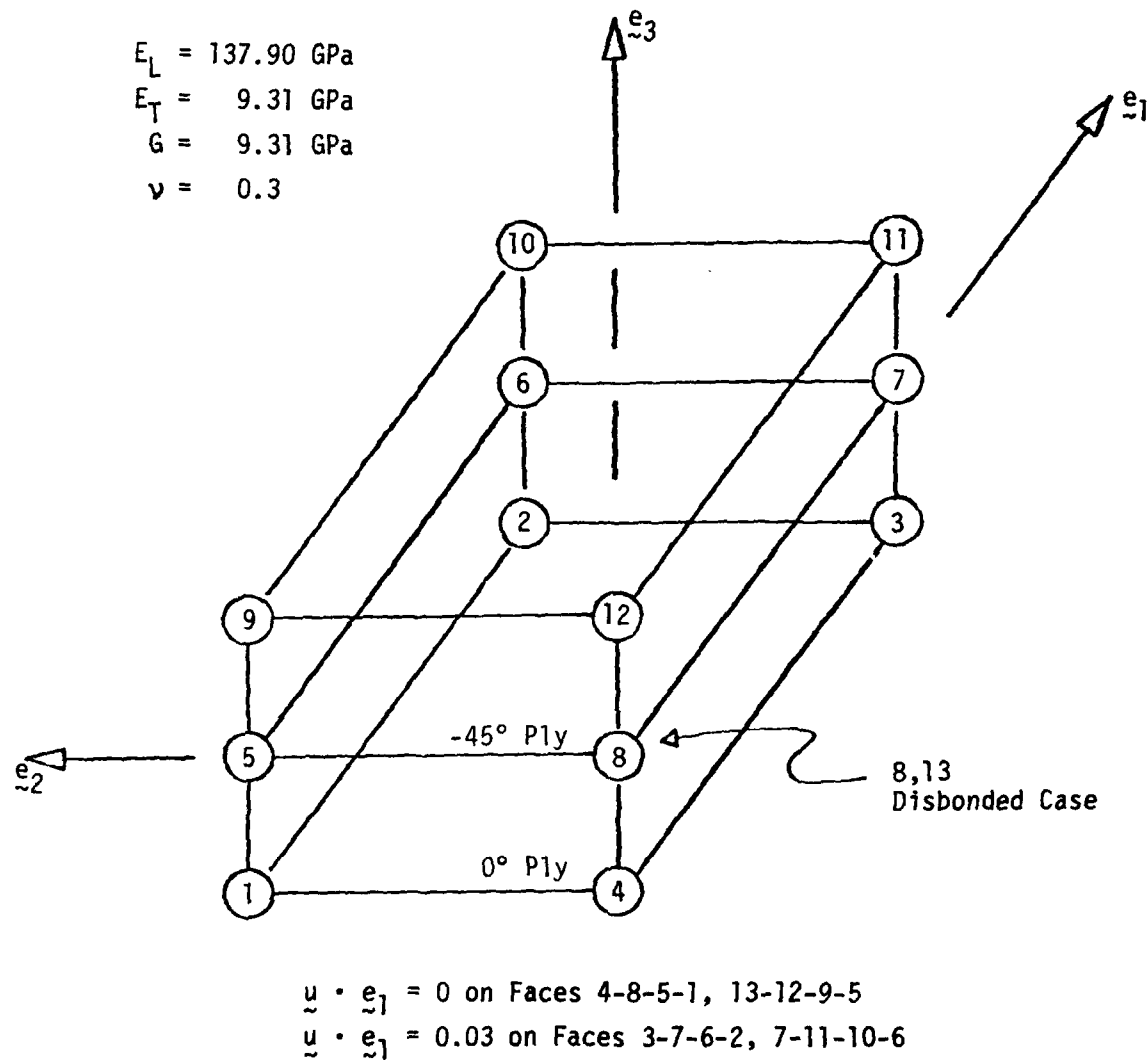


Figure 5. Two-Ply Disbond Prototype Model for Forces

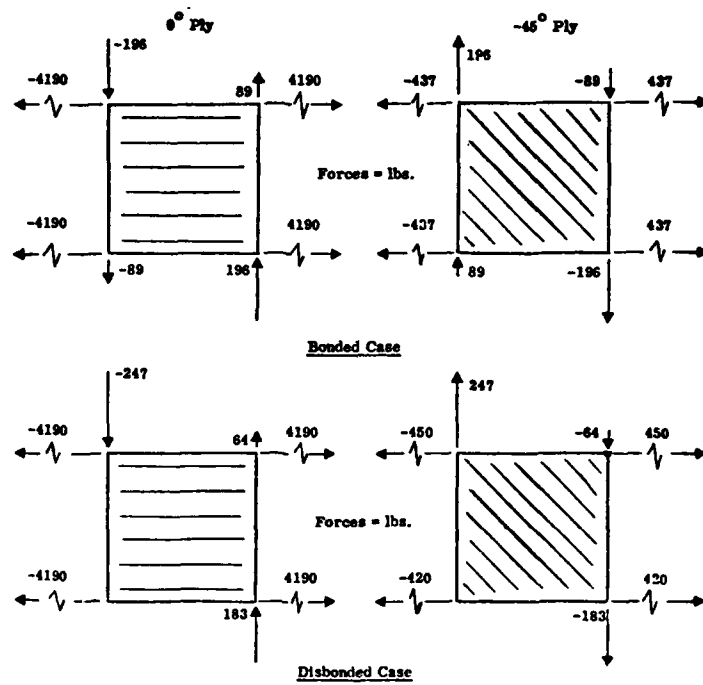


Figure 6. Interply Forces:  $[0/-45]$  Uniaxial Load

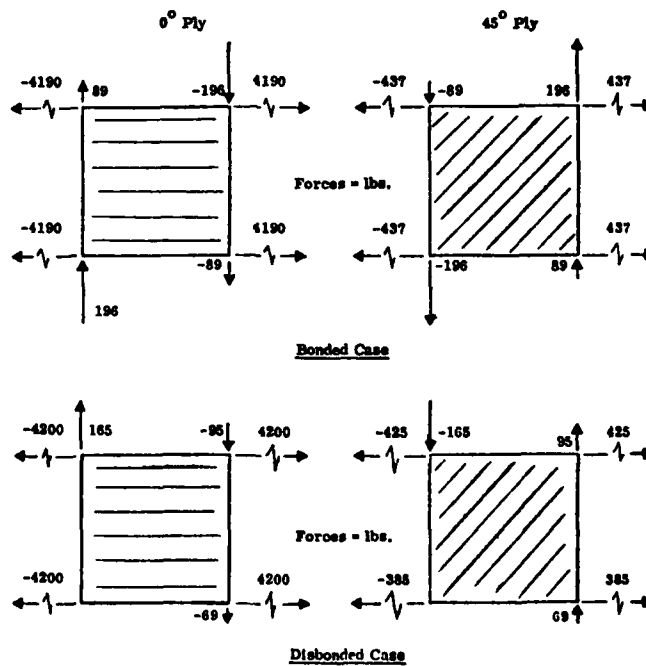


Figure 7. Interply Forces:  $[0/45]$  Uniaxial Load

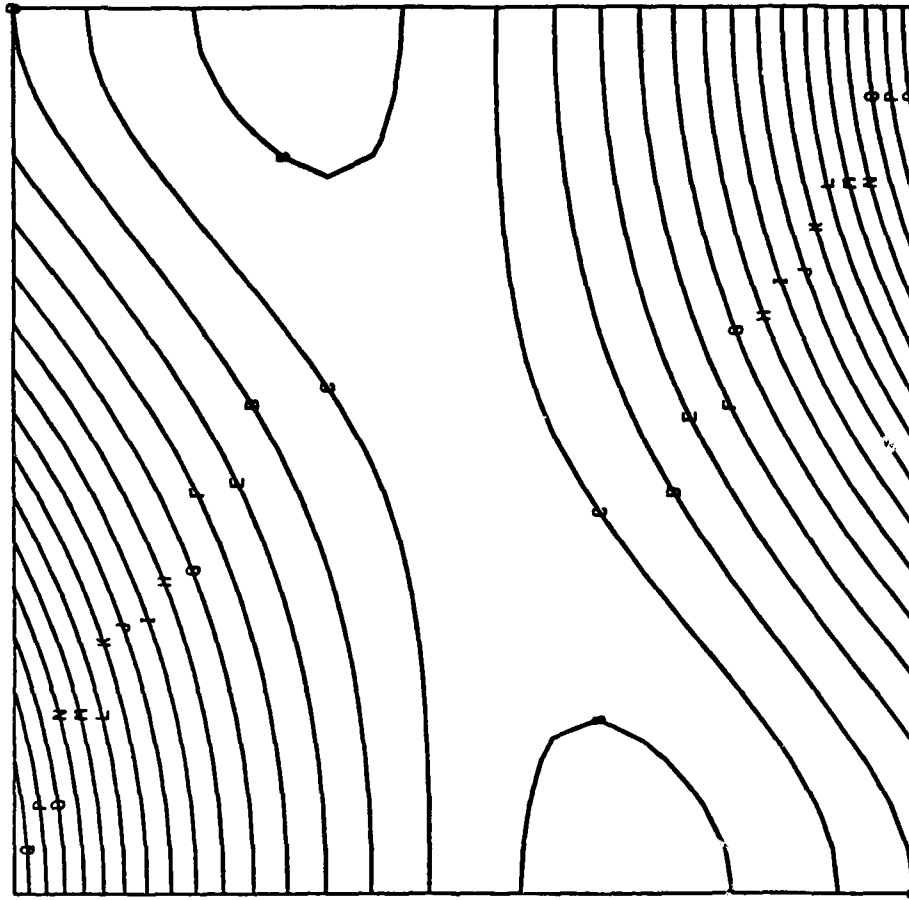
Next, a three-ply [0/45/-45] laminate model was used to examine out-of-plane warping under inplane loading of the unbalanced disbond material. Each ply was modeled with CCL elements, and the dimension of the square model was made equal the radius of the disbond. Under uniaxial load there is elastic coupling between stretching and twisting that caused large out-of-plane displacements because of the low bending stiffness of a three-ply laminate (the plies are only 0.01778 cm thick). The stresses, strains and deformations of this [0/45/-45] laminate are all either asymmetric or symmetric about axes at  $\pm 45^\circ$  to axes  $e_1$ ,  $e_2$ , Figure 8. These results and the [0/45] constraint force results indicate diagonal symmetry rather than Cartesian symmetry should be used in modeling force-deformation behavior of the disbanded laminate.

Another observation from the unbalanced prototype models was the extremely slow convergence of the conjugate-gradient solution procedure. The membrane response accounts for 99.7 percent of the potential energy and this result is converged in less than N cycles. However, the low energy out-of-plane bending response required almost 4N cycles to converge with little change to principal stresses or strains. Note that the interply normal forces are two orders of magnitude smaller than the inplane forces. The models were changed to CCC elements to check for purely numerical ill-conditioning and the same slow convergence was observed. No solution to the pathological computational behavior caused by weak out-of-plane coupling was found.

### 3.2 LAMINATE FINITE ELEMENT MODELS

The dimensions of the laminate were specified to insure no coupling between the displacement boundary conditions and deformations in the vicinity of the disbond. The laminate is square of width 15.24 cm (6 inches) with a disbond radius of 1.27 cm (.5-inch) between plies five and six, Figure 4. The plies are graphite-epoxy of thickness 0.01778 cm (0.007-inch) with their nominal elastic properties as given in Table 8. The stacking sequence for the laminate is [0,45,-45,0<sub>2</sub>,-45,45,0]<sub>T</sub> with the disbond between a 0° ply and a -45° ply. The edges are loaded by imposing a uniform inplane displacement of 0.00762 cm (0.003-inch) which produces biaxial compression.

A control model of the laminate was constructed using the same mesh in the  $Z_1, Z_2$  plane as in Figure 4, but with only four plies [0,45,-45,0]<sub>S</sub> through the half thickness. The purpose of this model was to provide before-and-after data for comparison with the disbanded results, in particular the



1 SURFACES OF UNDEFORMED GEOMETRY  
 DATA TYPE = DISPL COMPONENT 3  
 DATA IS IN THE CARTESIAN FRAME.  
 :N INEG = 1 NLINE = 1  
 NACCG = 3 NACCD = 3  
 VIEW = 0.00 0.00 0.00  
 ORIGIN = 0.00 0.00 10.00  
 ORTHOGRAPHIC PROJECTION  
 SYMMETRY OFF.  
 ALL LINES DRAWN

ELEMENT SET= 1  
 FACE SET= 6

18 CONTOUR INTERVALS  
 -.150000E-01(A) -.100000E-01(B)  
 -.500000E-02(C) 0.100000E-01(F)  
 .500000E-02(E) .100000E-01(F)  
 .150000E-01(G) .200000E-01(H)  
 .250000E-01(I) .300000E-01(J)  
 .350000E-01(K) .400000E-01(L)  
 .450000E-01(M) .500000E-01(N)  
 .550000E-01(O) .600000E-01(P)  
 .650000E-01(Q) .700000E-01(R)

UNBALANCED LAMINATE

Figure 8. Unbalanced Laminate Bending Displacements

TABLE 8. GRAPHITE-EPOXY NOMINAL ELASTIC PROPERTIES

$E_{11} = 137.90 \text{ GPa (20 msi)}$	$\nu_{12} = 0.3$	$G_{12} = 4.83 \text{ GPa (.7 msi)}$
$E_{22} = 9.31 \text{ GPa (1.35 msi)}$	$\nu_{13} = 0.3$	$G_{13} = 4.83 \text{ GPa (.7 msi)}$
$E_{33} = 9.31 \text{ GPa (1.35 msi)}$	$\nu_{23} = 0.3$	$G_{23} = 4.83 \text{ GPa (.7 msi)}$

internal forces. At the same time the control model shows the magnitude of the interlaminar constraint forces caused by the use of diagonal symmetry, Table 9. The forces  $F_2$  should be exactly zero if the interlaminar deformations are zero at the center of the laminate. Instead, a large self-equilibrating pair of forces occur between the  $0^\circ$  plies and the  $\pm 45^\circ$  plies. These forces distort the interlaminar stresses at the origin. It should be noted that  $F_2$  sums to zero between the +45 and -45 and the use of diagonal symmetry for these plies is consistent with material symmetry axes.

TABLE 9. BONDED LAMINATE CONSTRAINT FORCES THROUGH THE THICKNESS AT  $r = 0$ 

	$Z_3 = 4t_p$	$Z_3 = 3t_p$	$Z_3 = 2t_p$	$Z_3 = t_p$	$Z_3 = 0_p$
NODE	49	50	51	52	53
$F_1$	54.98 N	100.44 N	102.00 N	100.22 N	50.18 N
$F_2$	0.	43.41 N	0.	-43.41 N	0.

The control model also demonstrates that even the small biaxial strain ( $\epsilon \cong 0.1\%$ ) imposed at the edges of the panel is sufficient to buckle the laminate elastically. An engineering check was made using isotropic simply supported plate formulas with the stiff direction properties. This calculation indicates the laminate will buckle at  $P_1 = P_2 \cong 2000 \text{ N}$ , while the applied load is  $P > 10,000 \text{ N}$ . The exact solution for buckling of a laminated anisotropic plate [10] would be lower because the small number of plies accentuates the bending-stretching coupling. It seems likely that the disbond will reduce the buckling load even further or possibly cause a large deflection stability problem in a laminate this thin,  $T = 0.142 \text{ cm (0.056-inch)}$ .



### 3.3 DISBONDED LAMINATE RESULTS

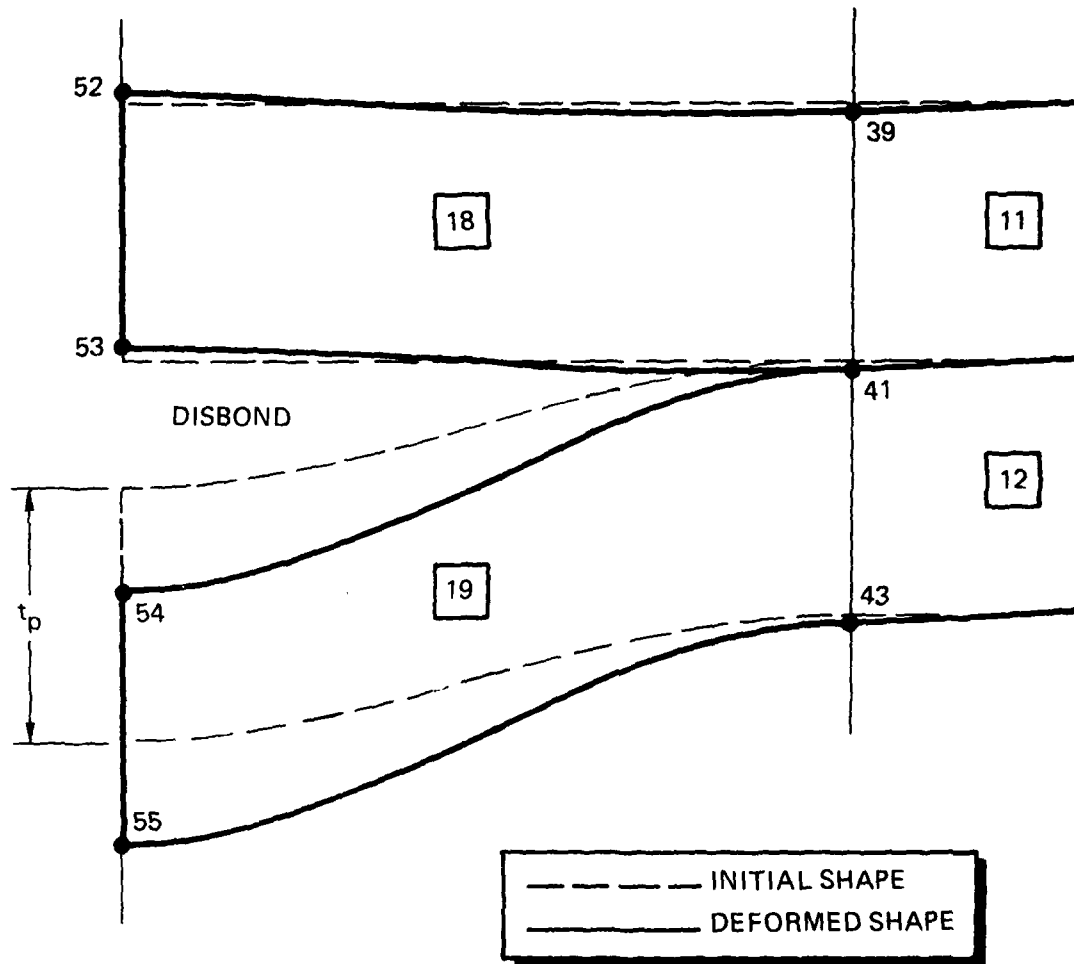
The effect of the disbond on the interlaminar force distribution is quite small and the effect on bending deformation is quite large. The centerpoint initial displacement caused by the disbond is  $0.5 t_p$  before any load is applied. The centerpoint elastic displacement after loading to a biaxial strain of only 0.1 percent is an additional  $0.4 t_p$ , Figure 9. In other words, a unit imposed displacement (biaxial) in the plane of the laminate produces almost a unit normal displacement at the center of the laminate. This result suggests the disbond will initially lead to a stiffness critical failure rather than a stress failure. The reason for this behavior seems to be the extremely low bending stiffness which produces large out-of-plane deformation when the disbond couples the membrane and bending displacement response. It is important to note that the potential energy change between the bonded and disbonded cases is less than one milli Joule, Table 10, which corresponds to an energy release rate of less than 1 N/m. In contrast, the critical energy release rate for an edge delamination, Reference 11, is well over 100 N/m for an 11 ply graphite-epoxy laminate.

TABLE 10. DISBONDED LAMINATE ENERGY CHANGE

Potential Energy		
Bonded	3.958455 Joules	(35.03528 in.-lbs)
Disbonded	3.958069 Joules	(35.03186 in.-lbs)

The small redistribution of internal forces is evident in Table 11 which shows the center point constraint forces through the thickness. Note that the forces at nodes 53 and 54 are summed when the disbond is closed. Note also that the force at node 53 in the bonded model must be added to node 52 for comparison with the disbond results. This is because only one element was used for the two center plies, Figure 4, in the disbond model. A check of the force changes through the thickness was also made at  $r = R$ , Table 12.

To a large extent the symmetry boundary conditions inhibit in-plane redistribution and to some extent interlaminar normal force changes. Considering the large normal displacements, Figure 9, one might expect an



8000393

Figure 9. Normal Deformations in the Plies Adjacent to the Disbond

TABLE 11. DISBONDED LAMINATE CONSTRAINT FORCE CHANGES THROUGH THE THICKNESS AT  $r = 0$ 

Node	Bonded			Disbonded		
	$Z_3$	$F_1$	$F_2$	$Z_3$	$F_1$	$F_2$
49	$4t_p$	54.98 N	0. N	$4t_p$	44.54 N	1.01 N
50	$3t_p$	100.44 N	43.41 N	$3t_p$	103.68 N	45.75 N
51	$2t_p$	102.00 N	0. N	$2t_p$	105.69 N	-.22 N
52	$t_p$	100.22 N	-43.41 N	$t_p$	160.78 N	-46.58 N
53*	0	50.18 N	0. N	$-t_p$	112.41 N	-.90 N
54				$-1.5 t_p$	43.62 N	-41.33 N
55		(Symmetric)		$-2.5 t_p$	90.67 N	3.22 N
56				$-3.5 t_p$	89.49 N	38.57 N
57				$-4.5 t_p$	42.46	1.43 N

\*Node 53 is at  $Z_3 = 0$  in the bonded laminate case.

interlaminar normal force to occur at  $r = R$ . As the data in Table 12 show, only a small increase in the small interlaminar normal force occurred at node 41. A possible explanation is that the symmetry boundary conditions at the center prevents nodes 53 and 54 from moving relative to each other in-plane as they probably would in a complete solution. If such deformations occur, they would create transverse shear gradients in-plane and equilibrium would require a normal stress gradient in the thickness direction,

$$\sigma_{31,1} + \sigma_{32,2} + \sigma_{33,3} = 0 \quad (3.2)$$

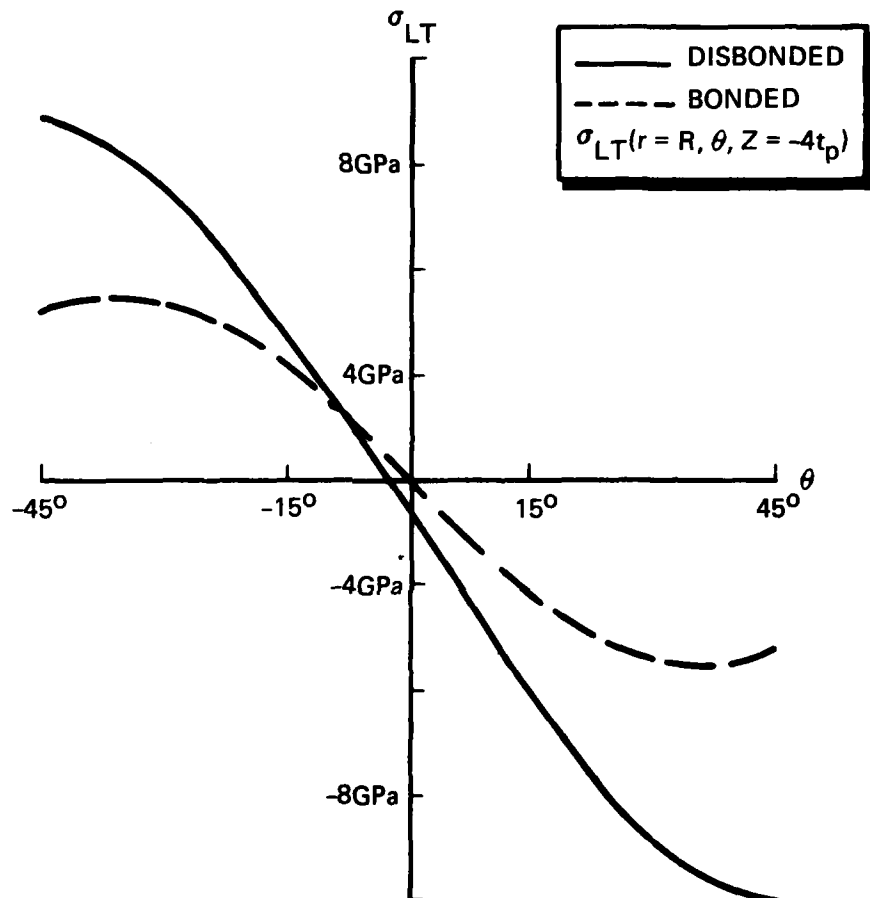
The magnitude of the spurious  $F_2$  force at node 54 suggests this deformation could be significant and would certainly increase the energy release rate. However, it would have to increase by a factor of 100 before the delamination would propagate if the data in Reference 11 apply. This uncertainty can only be resolved by analyzing a complete model without the assumption of symmetry conditions.

TABLE 12. DISBONDED LAMINATE CONSTRAINT FORCE CHANGES THROUGH THE THICKNESS AT  $r = R$ 

Node	Bonded			Disbonded		
	$Z_3$	$F_1 = F_2$	$F_3^*$	$Z_3$	$F_1 = F_2$	$F_3$
33	$4t_p$	12.18 N	0. N	$4t_p$	14.01 N	0. N
35	$3t_p$	74.54 N	$\pm 0.56$ N	$3t_p$	75.17 N	$\pm 0.07$ N
37	$2t_p$	68.29 N	$\pm 1.12$ N	$2t_p$	69.10 N	$\pm 0.14$ N
39	$t_p$	33.09 N	$\pm 0.84$ N	$t_p$	33.13 N	$\pm 0.93$ N
41	$-t_p$	(Symmetric)		$-t_p$	32.16 N	$\pm 1.49$ N
43	$-2t_p$			$-2t_p$	67.28 N	$\pm 0.84$ N
45	$-3t_p$			$-3t_p$	73.04 N	$\pm 0.34$ N
47	$-4t_p$			$-4t_p$	12.19 N	0. N

\* $F_3$  forces are self-equilibrating interlaminar forces.

The interlaminar stress results in keeping with the force results show only small changes in their distribution. On a percentage basis, the largest change occurs in the bottom ply where the small  $\sigma_{LT}$  shear stress is doubled. A plot of this stress component around the disbond at  $r = R$ , Figure 10, shows relative maximums and minimums at  $\pm 45^\circ$  as expected. The use of symmetry boundary conditions also caused local distortions at the origin in the stress results that make their magnitudes questionable. However, these conditions affect the bonded and disbonded cases equally.



8000394

Figure 10. Bottom Ply Shear Stress Changes

#### 4. LAMINATE IMPACT ANALYSES

At low velocities impact damage can be modeled as a quasi-static response problem using Hertzian contact pressures in most cases. This approach is used in the present study, and Greszczuk, Reference 12, gives an excellent account of the method and its rationale. The only analytic results available are for the elastic half space problem which was recently solved for a transversely isotropic material, Reference 13. One effect of transverse isotropy shown graphically in that paper is a shift of the maximum Von Mises stress from the impact centerline to a radius approaching the contact radius. The significance of this stress parameter for a composite is dubious, but it does indicate a trend of increasing transverse shear below the contact radius, which also occurs in the present results.

The disbanded laminate analysis problems caused by symmetry displacement boundary conditions led to the use of a full 360 degree finite element model for the impact problem. Another factor in this decision was the earlier PATCHES-III sandwich panel impact analysis [6] which also showed spurious constraint forces between the  $0^\circ$  and  $45^\circ$  plies on the centerline of a double symmetry model. In order to model a full 360 degrees, ply-by-ply, the program was modified to allow several hundred solid elements. Unfortunately, the computer budget available was sufficient to analyze only a 32 element model after all computational problems were resolved. These results, however, provide the first in-depth picture of the asymmetric interlaminar stress gradients that occur in a thick laminate impacted off-center. More detailed models were prepared for future analysis and these are in an appendix to this report.

##### 4.1 THICK LAMINATE COMPOSITE RESPONSE

A 48 ply graphite-epoxy laminate supported between two rigid spars is shown schematically in Figure 11 being impacted by a steel sphere. The impact point is close to a spar and in this problem a contact force of 4448 N was specified. Considering the large number of plies in this problem, not all plies can be modeled for any given analysis. This practical consideration becomes even more critical when symmetry conditions cannot be used. First a variable property 3D laminate model was used to determine the bending deformations in the vicinity of the impact site. This analysis used a large but finite width strip to avoid boundary condition effects, Figure 12. The 3D

laminates analysis produced large transverse shear stresses at the impact site approaching the bending stresses in magnitude. Laminates force-deformation properties were modeled using the  $C_{ij}^*(\xi)$  formulation derived earlier, Table 13. As these data indicate, only the off-diagonal coupling terms vary appreciably through the thickness.

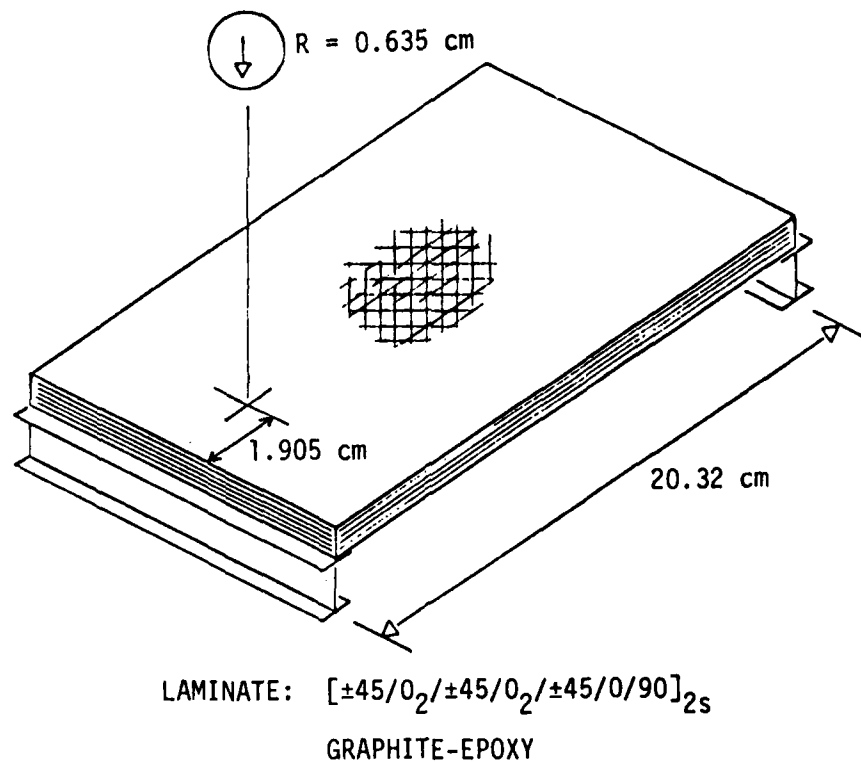
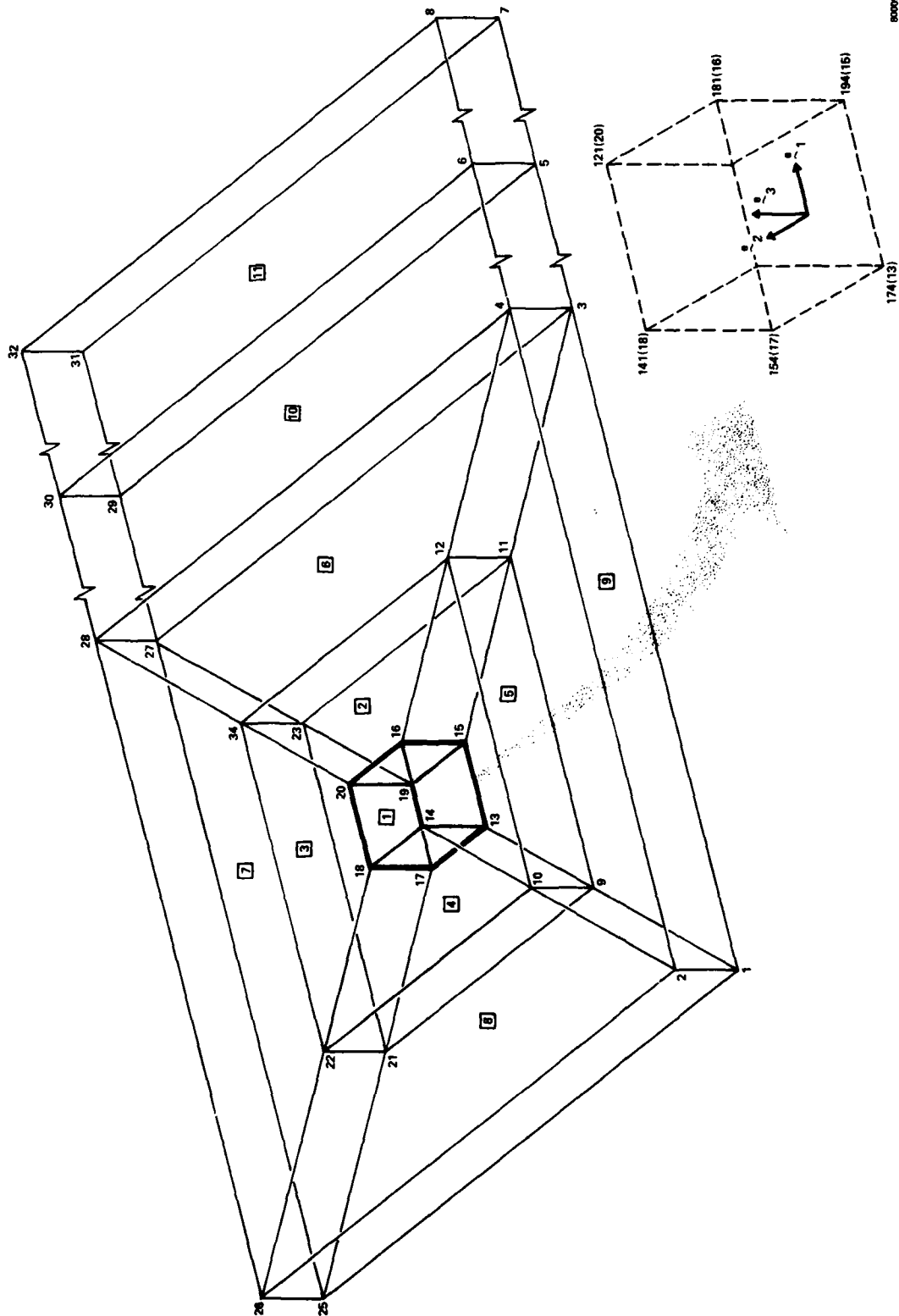


Figure 11. Thick Laminates Impact Schematic



8000630

Figure 12. Laminate Structural Response PATCHES-III Model



TABLE 13. PARAMETRIC CUBIC THICK LAMINATE PROPERTY MODEL\*

	$C_{ij}^*(0) = C_{ij}^*(1)$	$C_{ij}^*(1/3) = C_{ij}^*(2/3)$
C11	72.622	71.650
C12	21.712	14.906
C13	2.999	2.910
C14	2.427	-0.807
C22	24.173	36.887
C23	2.379	2.468
C24	2.427	-0.807
C33	9.432	9.432
C44	22.091	16.279
C55	3.771	3.771
C66	3.744	3.744

\*Stiffness in GPa units (1 Psi = 6894.757 Pascals)

#### 4.2 IMPACT SITE MODEL

The composite laminate displacement response for element number one, Figure 12, provided boundary conditions for the impact site model shown in Figure 13. The contact radius was determined using both the Greszczuk [12] equations and the Dahan and Zarka [13] equations. The latter have typographical errors that were reconciled using the limiting case of an isotropic half-space to yield

$$r_o = \left[ \frac{3FR}{2} \left( \frac{\delta_1 - \delta_2}{2} + \frac{1 - \nu^2}{E} \right) \right]^{1/3} \quad (4.1)$$

where  $\delta_1$  and  $\delta_2$  are lengthy algebraic functions of the half-space flexibilities  $S_{ij}^*$ . Substituting the laminate  $S_{ij}^*$  in these expressions gave

$$\delta_1 = -8.06 \times 10^{-12} \text{ m}^2/\text{N}$$

$$\delta_2 = -68.09 \times 10^{-12} \text{ m}^2/\text{N}$$

The remaining terms in Equation (4.1) are the force  $F = 4448 \text{ N}$ , the sphere



Figure 13. Impact Site PATCHES-III Model

radius  $R = 6.35$  mm and the elastic constants  $E = 206.84$  Gpa and  $\nu = 0.3$  for the sphere. These data produced a contact radius of  $r = 1.134$  mm. The Greszczuk equation for contact radius

$$r_o = \left[ \frac{3\pi}{4} FR (k_1 + k_2) \right]^{1/3} \quad (4.2)$$

also uses the  $S_{ij}^*$  to compute related coefficients  $k_1$  and  $k_2$  which are

$$k_1 = 1.4004 \times 10^{-12} \text{ m}^2/\text{N}$$

$$k_2 = 19.8173 \times 10^{-12} \text{ m}^2/\text{N}$$

producing a contact radius of 1.122 mm. The smaller radius was used to model the impact site so that  $T/R \cong 5.65$ .

Several disastrous attempts at analyzing the impact site model, Figure 13, were made using CCC elements for the upper plies and CCL elements for the subsurface laminate model. These attempts never quite converged and the deformations were highly distorted. After considerable effort it was determined that the model had pathological stiffness discontinuities in the thickness direction that were easily removed once found. At the impact site the elements through the thickness must be either all CCC or all CCL to avoid this condition. When the two element types are mixed under impact loading conditions, the CCC elements deform as if they were pressed against a rigid boundary. After resolving this modeling dilemma, excellent results were obtained using all CCC elements.

#### 4.3 INTERLAMINAR IMPACT STRESS RESULTS

It is important to keep in mind that the present results are for a small sphere impacting a thick laminate,  $T/R \cong 5.65$ , with sufficient energy to generate a contact force of 4448 N (1000 lbs). The resulting stress-strain gradients are quite high in the upper ply group, Figure 14, especially in material coordinates. Note in particular that the second ply, a - 45, has larger fiber stress gradients in the thickness direction than the top ply, although the magnitudes are slightly lower. The centerline Cartesian shear strains, Figure 15, show rather dramatically that the use of two symmetry planes would have produced large shear errors along the centerline. Interesting, the chordwise shear strain,  $\epsilon_{23}$ , is very small indicating one plane of symmetry

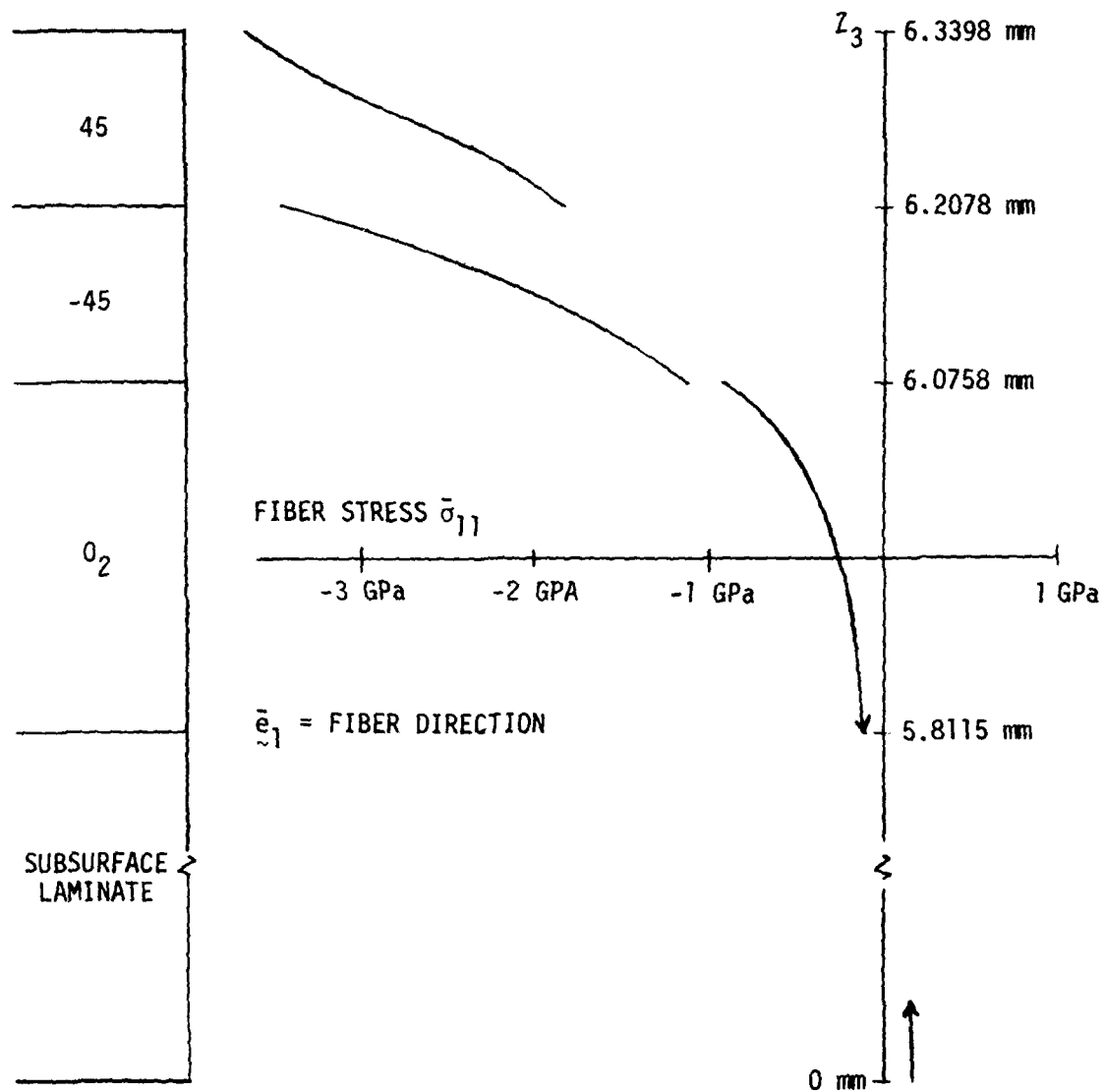


Figure 14. Centerline Fiber Stress

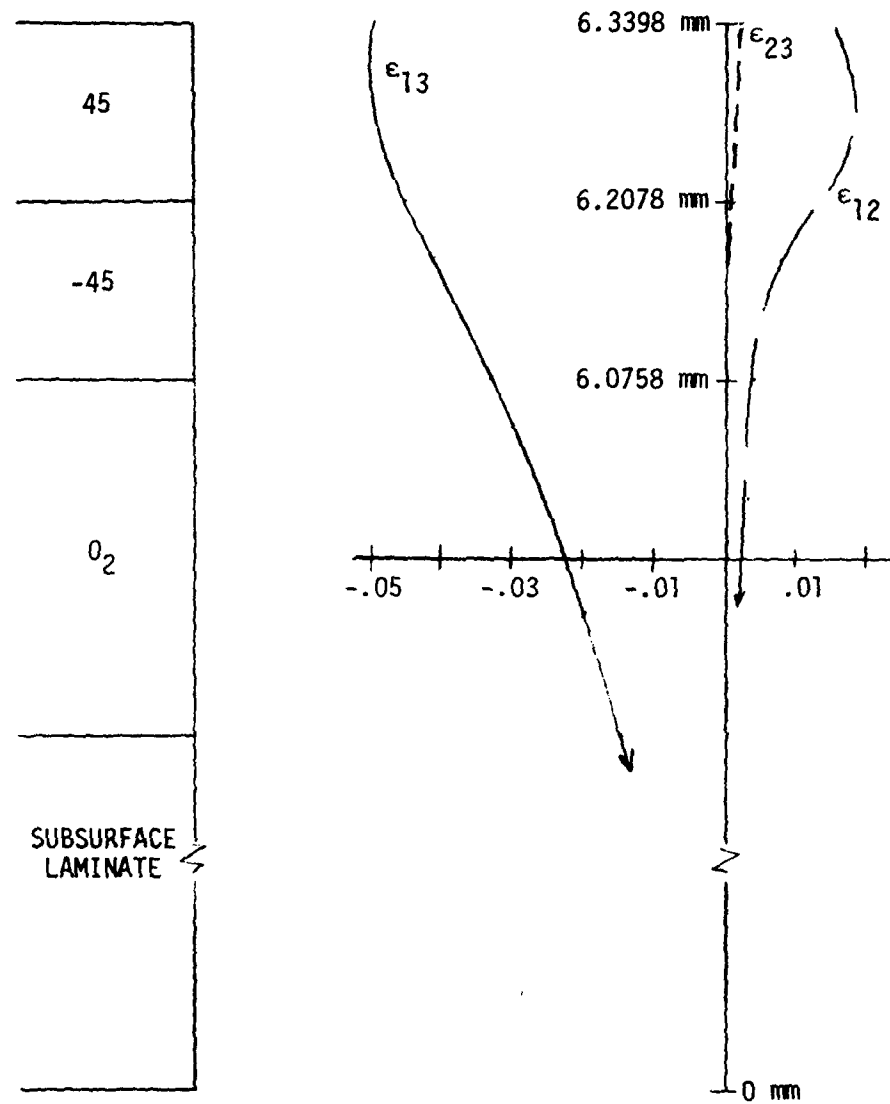


Figure 15. Cartesian Centerline Shear Strains

in the response. If the loading were not in the transverse direction, or if the laminate were unbalanced, even this symmetry condition would not exist.

Consider next the stress distribution around the perimeter of the impact site. The fiber stresses at the top surface as a function of circumferential position,  $\bar{\sigma}_{11}(\theta)$ , are shown in Figure 16. The tension stresses are confined to a thin layer at the free surface and are probably not a good indicator of actual fiber stresses. When the fiber stresses are averaged through a single ply thickness, Figure 16, the values are all compressive. In either case, the distribution is periodic in  $\theta$  with a period equal  $\pi$ . The distribution of transverse shear stress in material coordinates is also periodic, Figure 17, but with period equal  $2\pi$ . The two shear stress components in this figure,  $\bar{\sigma}_{13}$  and  $\bar{\sigma}_{23}$ , were averaged over one ply thickness, the second ply. This ply has the maximum transverse shear in the laminate and it occurs at the impact perimeter not the centerline. Similar behavior was observed by Dahan and Zarka in zinc and cadmium during elastic contact with a steel sphere. These materials also had their low stiffness in the direction normal to the impact surface, but they are not as anisotropic as the laminate material. It is also interesting to note that the two shear stress components  $\bar{\sigma}_{13}$  and  $\bar{\sigma}_{23}$  are phase shifted by  $90^\circ$  in the circumferential direction. The in-plane ply shear stress  $\bar{\sigma}_{12}$  in Figure 18 shows a quasi-periodic distribution of period equal  $\pi$  that is similar to the fiber stress distribution. However, the structural response of the laminate appears to be superimposed on the elastic half-space response. This would explain the  $\bar{\sigma}_{12}$  peak nearest the center of the laminate being slightly smaller. There is also a subharmonic component that may be caused by the composite solution boundary conditions applied to the impact site model. To explore this second order effect would require additional analyses. A summary of the ply material stress maximums is provided in Table 14.

It is interesting to observe the similarities and differences in a 3D laminate solution and a 3D elasticity solution in the impact area. The deformations at the top surface are compared in Figure 19 and show very similar shapes. The maximum 3D laminate displacement is about 85 percent of the elasticity result; however, the laminate strains are an order of magnitude too low at the top surface. The elasticity solution using laminate properties was much closer but still low. The normal strain in this case is quite close, but the in-plane strains are one-half to one-third the ply strain results.

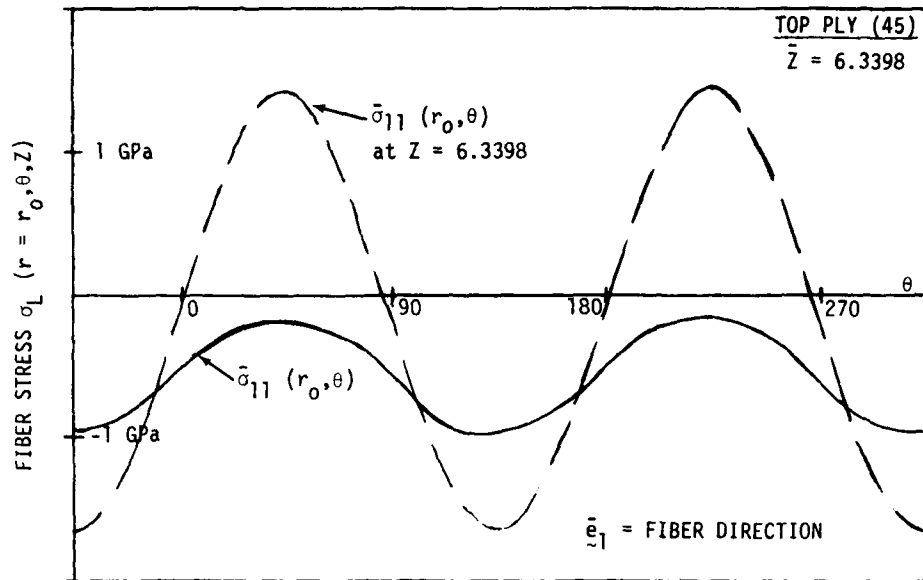


Figure 16. Fiber Stresses Around Impact Perimeter

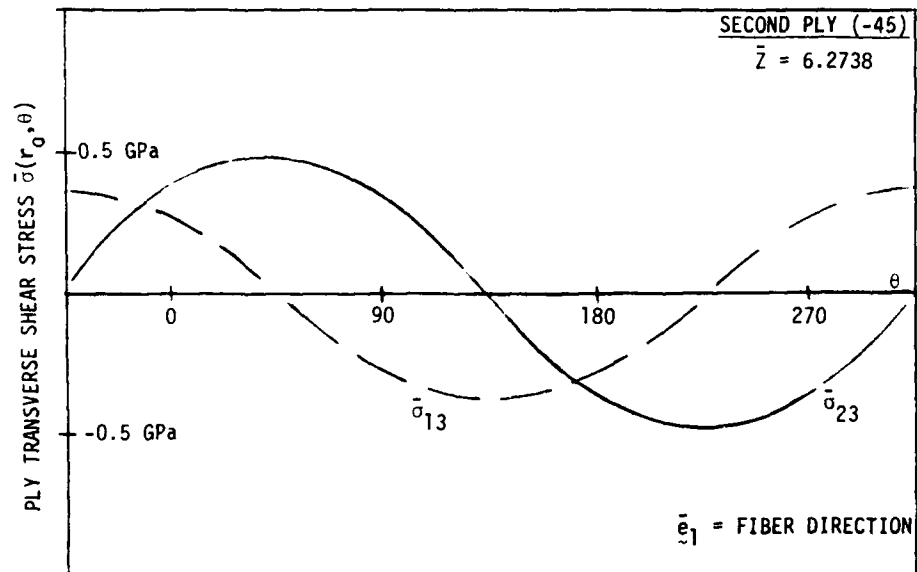


Figure 17. Transverse Shear Stresses Around Impact Perimeter

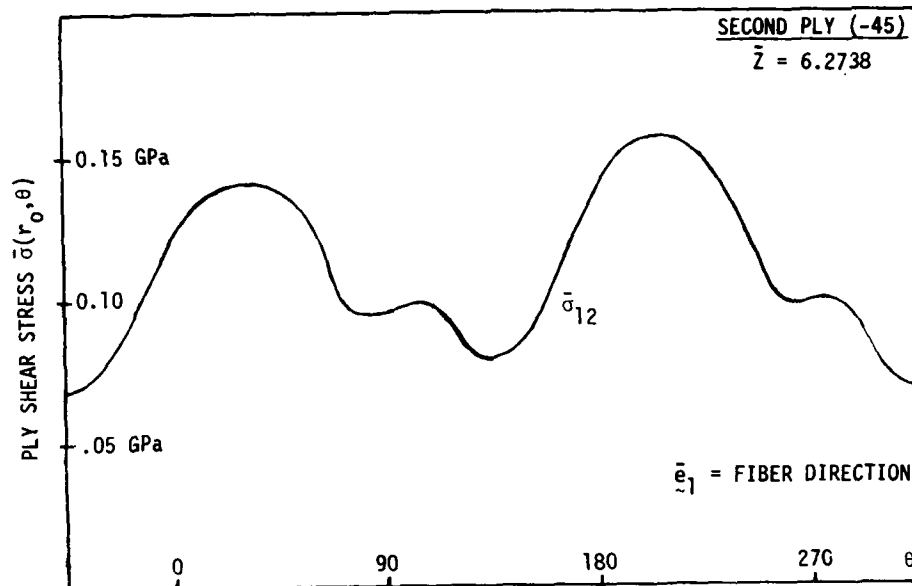


Figure 18. Ply Shear Stress Around Impact Perimeter

TABLE 14. THICK LAMINATE PLY STRESS SUMMARY

	$\sigma_L$	$\sigma_T$	$\sigma_{LT}$	$\sigma_{TT}$
$\sigma/P_0$	2.05	.99	.28	-.28
Node	1	1	22,62	22,62



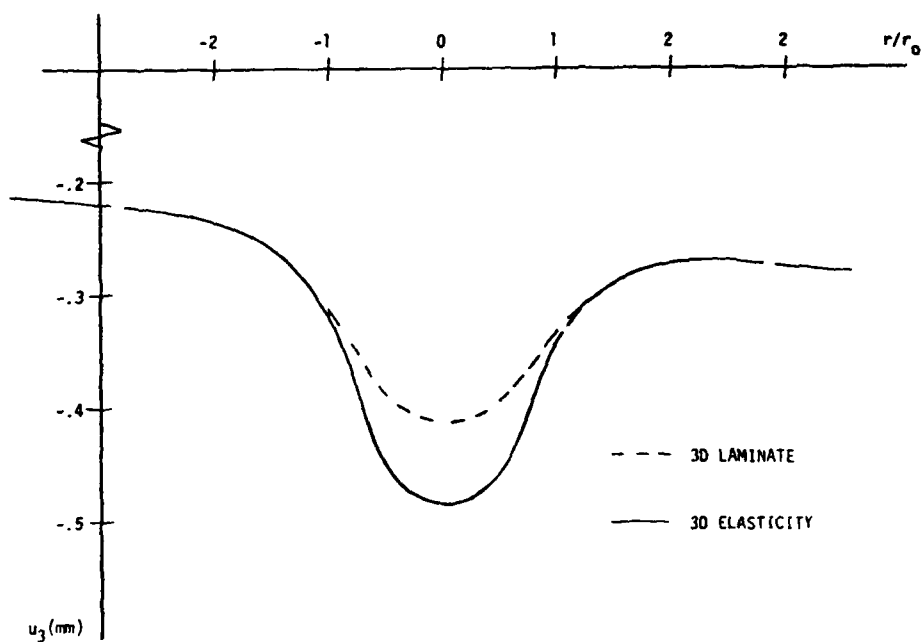


Figure 19. Thick Laminate Local Bending Deformation Comparisons

## 5. CONCLUSIONS AND RECOMMENDATIONS

A systematic approach to modeling complex interlaminar stress gradients has been developed and applied to two graphite-epoxy laminates. The approach uses variable property 3D finite elements that correctly model force-deformation behavior and constant property 3D finite elements that accurately model ply shear strains. Analyses for this class of problems are difficult, but considerable progress has been made toward solving the computational and modeling issues encountered.

- To model composite laminate force-deformation behavior with 3D finite elements requires, in general, properties that vary through the laminate thickness.
- Interlaminar deformations are not symmetric in a balanced symmetric laminate under symmetric in-plane loads.
- Interlaminar deformations have one plane of symmetry in a balanced symmetric laminate under normal Hertzian contact pressure.

Analysis of the disbanded laminate force deformation behavior indicates a large out-of-plane displacement response occurs without significant internal force redistribution. Comparison with a bonded laminate control model also indicates very little energy is released by the disbond. The new CCL finite element worked well in this application and should be an effective new tool for analyzing interlaminar force-deformation behavior in the vicinity of defects. It is interesting to note that more accurate results can be obtained on reanalysis by simply changing the element specification to CCC as in the P-Version of the finite element method [14].

Analysis of the thick laminate impacted off-center by a small sphere indicates the maximum transverse shear occurs below the surface in the second ply for the  $[\pm 45/0_2/\pm 45/0_2/\pm 45/0/90]_{2S}$  layup. This maximum occurs at the contact radius and both transverse shears in material coordinates have a sinusoidal variation around the perimeter. The fiber stresses also vary sinusoidally, but with one-half the period of the transverse shears. Only the in-plane shear stress shows a noticeable effect of the impact site being off-center. The edge closest the spar boundary has slightly higher ply shear. This also occurs in the ply shear strains with the relative increase being

on the order of 10 percent. These results were obtained after several analysis failures caused by mixing CCL and CCC elements in the thickness direction. Based on these results and those from the disbanded laminate the following additional analyses are recommended:

- Analyze the disbanded laminate without any symmetry assumptions.
- Analyze the disbanded laminate with twice as many plies,  $[0/\pm 45/0_2/\pm 45/0]_{2S}$ , with the disbond in the same location.
- Analyze the impact site with the focus on the bottom ply group.

Now that accurate modeling techniques for finite element analysis of interlaminar behavior have been developed, a combined test/analysis study of the effects of defects is recommended. It would be possible to evaluate energy release rate and possibly other parameters as a measure of how large a delamination can become before unstable propagation takes place. Pre-test analyses could be used to define the critical load conditions and to help locate instrumentation. In order to facilitate this work it would be desirable to interface the PATCHES-III program with a composite material synthesis program [15], [16] for pre- and postprocessing of the finite element results. This would allow basic ply properties and layup data as input and automate the recovery of ply stress-strain data from composite stress-strain results. It would also allow Tsai-Wu, Hill and other failure criteria to be applied to the PATCHES-III results.

## 6. REFERENCES

1. Spilker, R. L., S. C. Chou, and O. Orringer, "Alternate Hybrid-Stress Elements for Analysis of Multilayer Composite Plates," J. Composite Materials, Vol. 11, pp. 51-70, 1977.
2. Wang, A. S. D. and F. W. Crossman, "Calculation of Edge Stresses in Multi-Layer Laminates by Sub-Structuring," J. Composite Materials, Vol. 12, pp. 76-83, 1978.
3. Pagano, N. J., "Stress Fields in Composite Laminates," AFML TR-77-14, Air Force Materials Laboratory, 1977.
4. Pagano, N. J., "Exact Moduli of Anisotropic Laminates," Composite Materials, Vol. 2, edited by G. P. Sendeckyj, pp. 23-44.
5. Stanton, E. L., "A General Three-Dimensional Computational Model for Nonlinear Composite Structures and Materials," AIAA Paper No. 77-360, in Proceedings AIAA/ASME/SAE 18th SDM Conference, pp. 9-22, 1977.
6. Stanton, E. L. and L. M. Crain, "Application of PATCHES-III to the Three-Dimensional Response of Laminated Composites," NADC Contract N62269-75-C-0438, Final Report, 1975.
7. Kibler, J. J. and S. N. Chatterjee, "Development of Minimechanics Model for 3D Carbon/Carbon Materials," Materials Science Corp., Report TFR 7510, 1975.
8. Williams, J. G., et al., "Recent Developments in the Design Testing and Impact-Damage Tolerance of Stiffened Composite Panels, NASA TM-80077, April 1979.
9. Williams, J. G., et al., "Low-Velocity Impact Damage in Graphite-Fiber Reinforced Epoxy Laminates," Presented at the 34th Annual SAMPE Conference, New Orleans, 1979.
10. Whitney, J. M. and A. W. Leissa, "Analysis of a Simply Supported Laminated Anisotropic Rectangular Plate," AIAA Journal, Vol. 8, pp. 28-38, 1970.
11. Rybicki, E. F., et al., "An Energy Release Rate Approach for Stable Crack Growth in the Free-Edge Effect Delamination Problem," J. Composite Materials, Vol. 11, pp. 470-487, 1977.
12. Greszczuk, L. B., et al., "Investigation of Brittle Fractures in Graphite Epoxy Composites Subjected to Impact," USAAMRDL-TR-75-15 (AD-A012-269), May 1975.
13. Dahan, M. and J. Zarka, "Elastic Contact Between a Sphere and a Semi Infinite Transversely Isotropic Body," Int. J. Solids Structures, Vol. 13, pp. 229-238, 1977.

14. Babuska, I., et al., "The P-Version of the Finite Element Method," Washington University, Report No. WU/CCM-79/1, May 1979.
15. Chamis, C. C., "Computerized Multilevel Analysis for Multilayered Fiber Composites," Computers and Structures, Vol. 3, pp. 467-482, 1973.
16. Stanton, E. L. and L. M. Crain, "Advances in Parametric Cubic Modeling for Finite Element Data Generation," Proceedings Second World Finite Element Conference, Bournemouth, England, pp. 386-496, 1978.

## APPENDIX

The PATCHES-III input data for the two laminates analyzed in this report and data modifications necessary to analyze three additional impact cases, Table A-1, are provided in this appendix. The structural response model that provides displacement boundary conditions for the impact site model is included for each case. Also, a schematic of a more detailed model of the impact site that includes the entire 12 plies in the basic repeating ply group is provided.

TABLE A-1. PATCHES-III LAMINATE IMPACT CASES

Case	Impact Site	Sphere Radius	Contact Radius	Status
1	Z1 = 1.91 cm	0.635 cm	1.12 mm	Analyzed
2	Z1 = 1.91 cm	2.540 cm	1.78 mm	Modeled
3	Z1 = 10.16 cm	0.635 cm	1.12 mm	Modeled
4	Z1 = 10.16 cm	2.540 cm	1.78 mm	Modeled

NADC-80135-60

PATCHES-III INPUT DATA  
DISBONDED LAMINATE MODEL

**A-3**

**VERSION 8.2C**



10.32.16. 12/21/77

CASE CONTROL DATA

TITLE = DISORD LAMINATE CASE  
 SUBTITLE = SYMMETRY BOUNDARY CONDITIONS  
 TIME = 14  
 SDC = 10  
 CHRPNT = ELEMENT.CG  
 OUTPUT  
 EVERYTHING  
 BEGIN ALLK

CAPD FIELD-1, FIELD-2, FIELD-3, FIELD-4, FIELD-5, FIELD-6, FIELD-7, FIELD-8, FIELD-9, FIELD-10

1-	CPDE3	1	19	20	4	3	+C1
2-	+C1	CC1*	17	18	2	1	
3-	CPDE3	2	21	22	6	5	+C2
4-	+C2	CC1*	19	20	4	3	
5-	CPDE3	3	23	24	8	7	+C3
6-	+C3	CC1*	21	22	6	5	
7-	CPDE3	4	25	26	10	9	+C4
8-	+C4	CC1*	23	24	8	7	
9-	CPDE3	5	27	28	12	11	+C5
10-	+C5	CC1*	25	26	10	9	
11-	CPDE3	6	29	30	14	13	+C6
12-	+C6	CC1*	27	28	12	11	
13-	CPDE3	7	31	32	16	15	+C7
14-	+C7	CC1*	29	30	14	13	
15-	CPDE3	8	35	36	20	19	+C8
16-	+C8	CC1*	33	34	18	17	
17-	CPDE3	9	37	38	22	21	+C9
18-	+C9	CC1*	35	36	20	19	
19-	CPDE3	10	39	40	24	23	+C10
20-	+C10	CC1*	37	38	22	21	
21-	CPDE3	11	41	42	26	25	+C11
22-	+C11	CC1*	39	40	24	23	
23-	CPDE3	12	43	44	28	27	+C12
24-	+C12	CC1*	41	42	26	25	
25-	CPDE3	13	45	46	30	29	+C13
26-	+C13	CC1*	43	44	28	27	
27-	CPDE3	14	47	48	32	31	+C14
28-	+C14	CC1*	45	46	30	29	
29-	CPDE3	15	50	50	36	35	+C15
30-	+C15	CC1*	49	49	34	33	
31-	CPDE3	16	51	51	38	37	+C16
32-	+C16	CC1*	50	50	36	35	
33-	CPDE3	17	52	52	40	39	+C17
34-	+C17	CC1*	51	51	38	37	
35-	CPDE3	18	53	53	42	41	+C18
36-	+C18	CC1*	52	52	40	39	
37-	CPDE3	19	55	55	44	43	+C19
38-	+C19	CC1*	54	54	42	41	
39-	CPDE3	20	56	56	46	45	+C20
40-	+C20	CC1*	55	55	44	43	
41-	CPDE3	21	57	57	48	47	+C21
42-	+C21	CC1*	56	56	46	45	
43-	HP2PAT	1	2	1			
44-	HP2PAT	2	3	2			
45-	HP2PAT	3	4	3			
46-	HP2PAT	4	5	4			

FIELD-1, FIELD-2, FIELD-3, FIELD-4, FIELD-5, FIELD-6, FIELD-7, FIELD-8, FIELD-9, FIELD-10  
CAPU

NAD C-80135-60

**A-6**

CARD FIELD-1, FIELD-2, FIELD-3, FIELD-4, FIELD-5, FIELD-6, FIELD-7, FIELD-8, FIELD-9, FIELD-10

12X-37	-021	-021	-021	+M37
+M37				

4124-30	-0.020	-0.026	+H30
4125-30	-0.020	-0.020	+H30

IRX-61	- .6105	- .007	- .000366	- .0105	- .007	- .000366	- .000366	+M41
--------	---------	--------	-----------	---------	--------	-----------	-----------	------

194X-42 -.0175 -.000366-.0175 -.0140 -.000366-.000366+M42

442	1000-43	-0245	-0210	-000366-	-0210	-000366-	-000366+M43
-----	---------	-------	-------	----------	-------	----------	-------------

443	44	000366-	0315	0280	000366-	000366+M44
443	44	000366-	0315	0280	000366-	000366+M44

1	8	11	21	31
PATCH				
*****				

PAICH	2	8	11	21	32
PAICH	3	8	11	21	33

PATCH	4	8	11	21	34
PATCH	5	8	11	21	35

PATCH	6	11	21	36
PATCH	7	11	21	37
S	9	11	21	38

DATE	NO.	NAME	AMOUNT	TOTAL
1914	23	H. H. H.	11	21
1914	24	H. H. H.	12	33
1914	25	H. H. H.	12	45
1914	26	H. H. H.	12	57
1914	27	H. H. H.	12	69
1914	28	H. H. H.	12	81
1914	29	H. H. H.	12	93
1914	30	H. H. H.	12	105
1914	31	H. H. H.	12	117
1914	32	H. H. H.	12	129
1914	33	H. H. H.	12	141
1914	34	H. H. H.	12	153
1914	35	H. H. H.	12	165
1914	36	H. H. H.	12	177
1914	37	H. H. H.	12	189
1914	38	H. H. H.	12	201
1914	39	H. H. H.	12	213
1914	40	H. H. H.	12	225
1914	41	H. H. H.	12	237
1914	42	H. H. H.	12	249
1914	43	H. H. H.	12	261
1914	44	H. H. H.	12	273
1914	45	H. H. H.	12	285
1914	46	H. H. H.	12	297
1914	47	H. H. H.	12	309
1914	48	H. H. H.	12	321
1914	49	H. H. H.	12	333
1914	50	H. H. H.	12	345
1914	51	H. H. H.	12	357
1914	52	H. H. H.	12	369
1914	53	H. H. H.	12	381
1914	54	H. H. H.	12	393
1914	55	H. H. H.	12	405
1914	56	H. H. H.	12	417
1914	57	H. H. H.	12	429
1914	58	H. H. H.	12	441
1914	59	H. H. H.	12	453
1914	60	H. H. H.	12	465
1914	61	H. H. H.	12	477
1914	62	H. H. H.	12	489
1914	63	H. H. H.	12	501
1914	64	H. H. H.	12	513
1914	65	H. H. H.	12	525
1914	66	H. H. H.	12	537
1914	67	H. H. H.	12	549
1914	68	H. H. H.	12	561
1914	69	H. H. H.	12	573
1914	70	H. H. H.	12	585
1914	71	H. H. H.	12	597
1914	72	H. H. H.	12	609
1914	73	H. H. H.	12	621
1914	74	H. H. H.	12	633
1914	75	H. H. H.	12	645
1914	76	H. H. H.	12	657
1914	77	H. H. H.	12	669
1914	78	H. H. H.	12	681
1914	79	H. H. H.	12	693
1914	80	H. H. H.	12	705
1914	81	H. H. H.	12	717
1914	82	H. H. H.	12	729
1914	83	H. H. H.	12	741
1914	84	H. H. H.	12	753
1914	85	H. H. H.	12	765
1914	86	H. H. H.	12	777
1914	87	H. H. H.	12	789
1914	88	H. H. H.	12	801
1914	89	H. H. H.	12	813
1914	90	H. H. H.	12	825
1914	91	H. H. H.	12	837
1914	92	H. H. H.	12	849
1914	93	H. H. H.	12	861
1914	94	H. H. H.	12	873
1914	95	H. H. H.	12	885
1914	96	H. H. H.	12	897
1914	97	H. H. H.	12	909
1914	98	H. H. H.	12	921
1914	99	H. H. H.	12	933
1914	100	H. H. H.	12	

4	H	12	22	32
5	H	12	22	32
6	H	12	22	32
7	H	12	22	32
8	H	12	22	32
9	H	12	22	32
10	H	12	22	32
11	H	12	22	32
12	H	12	22	32
13	H	12	22	32
14	H	12	22	32
15	H	12	22	32
16	H	12	22	32
17	H	12	22	32
18	H	12	22	32
19	H	12	22	32
20	H	12	22	32
21	H	12	22	32
22	H	12	22	32
23	H	12	22	32
24	H	12	22	32
25	H	12	22	32
26	H	12	22	32
27	H	12	22	32
28	H	12	22	32
29	H	12	22	32
30	H	12	22	32
31	H	12	22	32
32	H	12	22	32
33	H	12	22	32
34	H	12	22	32
35	H	12	22	32
36	H	12	22	32
37	H	12	22	32
38	H	12	22	32
39	H	12	22	32
40	H	12	22	32
41	H	12	22	32
42	H	12	22	32
43	H	12	22	32
44	H	12	22	32
45	H	12	22	32
46	H	12	22	32
47	H	12	22	32
48	H	12	22	32
49	H	12	22	32
50	H	12	22	32
51	H	12	22	32
52	H	12	22	32
53	H	12	22	32
54	H	12	22	32
55	H	12	22	32
56	H	12	22	32
57	H	12	22	32
58	H	12	22	32
59	H	12	22	32
60	H	12	22	32
61	H	12	22	32
62	H	12	22	32
63	H	12	22	32
64	H	12	22	32
65	H	12	22	32
66	H	12	22	32
67	H	12	22	32
68	H	12	22	32
69	H	12	22	32
70	H	12	22	32
71	H	12	22	32
72	H	12	22	32
73	H	12	22	32
74	H	12	22	32
75	H	12	22	32
76	H	12	22	32
77	H	12	22	32
78	H	12	22	32
79	H	12	22	32
80	H	12	22	32
81	H	12	22	32
82	H	12	22	32
83	H	12	22	32
84	H	12	22	32
85	H	12	22	32
86	H	12	22	32
87	H	12	22	32
88	H	12	22	32
89	H	12	22	32
90	H	12	22	32
91	H	12	22	32
92	H	12	22	32
93	H	12	22	32
94	H	12	22	32

11	BATCH	9	12	22	34
12	BATCH	9	12	22	35
13	BATCH	8	10	22	37

DATE	TIME	PLACE	REMARKS
12	12	12	37
14	8	12	22
24	8	12	22
24	8	12	22

24	B	12	22	38
BATCH				
15	B	13	23	31
BATCH				
14	B	12	22	30
BATCH				

15	8	13	32
16	8	23	33
17	8	23	34
18	8	13	35
19	8	13	36
20	8	13	37
21	8	13	38
22	8	13	39
23	8	13	40
24	8	13	41
25	8	13	42
26	8	13	43
27	8	13	44
28	8	13	45
29	8	13	46
30	8	13	47
31	8	13	48
32	8	13	49
33	8	13	50
34	8	13	51
35	8	13	52
36	8	13	53
37	8	13	54
38	8	13	55
39	8	13	56
40	8	13	57
41	8	13	58
42	8	13	59
43	8	13	60
44	8	13	61
45	8	13	62
46	8	13	63
47	8	13	64
48	8	13	65
49	8	13	66
50	8	13	67
51	8	13	68
52	8	13	69
53	8	13	70
54	8	13	71
55	8	13	72
56	8	13	73
57	8	13	74
58	8	13	75
59	8	13	76
60	8	13	77
61	8	13	78
62	8	13	79
63	8	13	80
64	8	13	81
65	8	13	82
66	8	13	83
67	8	13	84
68	8	13	85
69	8	13	86
70	8	13	87
71	8	13	88
72	8	13	89
73	8	13	90
74	8	13	91
75	8	13	92
76	8	13	93
77	8	13	94
78	8	13	95
79	8	13	96
80	8	13	97
81	8	13	98
82	8	13	99
83	8	13	100
84	8	13	101
85	8	13	102
86	8	13	103
87	8	13	104
88	8	13	105
89	8	13	106
90	8	13	107
91	8	13	108
92	8	13	109
93	8	13	110
94	8	13	111
95	8	13	112
96	8	13	113
97	8	13	114
98	8	13	115
99	8	13	116
100	8	13	117
101	8	13	118
102	8	13	119
103	8	13	120
104	8	13	121
105	8	13	122
106	8	13	123
107	8	13	124
108	8	13	125
109	8	13	126
110	8	13	127
111	8	13	128
112	8	13	129
113	8	13	130
114	8	13	131
115	8	13	132
116	8	13	133
117	8	13	134
118	8	13	135
119	8	13	136
120	8	13	137

DATE	TIME	LOCATION	WIND	WAVE	SEA	TEMP	WIND	WAVE	SEA	TEMP
1	0	13	22	13	35					
2	8	13	22	13	35					
3	8	13	22	13	35					
4	8	13	22	13	35					
5	8	13	22	13	35					
6	8	13	22	13	35					
7	8	13	22	13	35					
8	8	13	22	13	35					
9	8	13	22	13	35					
10	8	13	22	13	35					
11	8	13	22	13	35					
12	8	13	22	13	35					
13	8	13	22	13	35					
14	8	13	22	13	35					
15	8	13	22	13	35					
16	8	13	22	13	35					
17	8	13	22	13	35					
18	8	13	22	13	35					
19	8	13	22	13	35					
20	8	13	22	13	35					
21	8	13	22	13	35					
22	8	13	22	13	35					
23	8	13	22	13	35					
24	8	13	22	13	35					
25	8	13	22	13	35					
26	8	13	22	13	35					
27	8	13	22	13	35					
28	8	13	22	13	35					
29	8	13	22	13	35					
30	8	13	22	13	35					
31	8	13	22	13	35					
32	8	13	22	13	35					
33	8	13	22	13	35					
34	8	13	22	13	35					
35	8	13	22	13	35					
36	8	13	22	13	35					
37	8	13	22	13	35					
38	8	13	22	13	35					
39	8	13	22	13	35					
40	8	13	22	13	35					
41	8	13	22	13	35					
42	8	13	22	13	35					
43	8	13	22	13	35					
44	8	13	22	13	35					
45	8	13	22	13	35					
46	8	13	22	13	35					
47	8	13	22	13	35					
48	8	13	22	13	35					
49	8	13	22	13	35					
50	8	13	22	13	35					
51	8	13	22	13	35					

ATCH	17	0	13	23	41
ATCH	20	8	13	23	42
ATCH	21	8	13	23	43

DATE	TIME	LOCATION	WIND	WAVE	SEA	TEMP	WIND	WAVE	SEA	TEMP
22	25	13	8	13	23	44				
23	13	23	44							
24	13	23	44							
25	13	23	44							
26	13	23	44							
27	13	23	44							
28	13	23	44							
29	13	23	44							
30	13	23	44							
31	13	23	44							

2	1	45.0
2	1	-45.0

4	1	PPF3	0.
5	1	PPF3	-45.

[illegible]

1	40E3	8	0.
1	40E3	9	45.

---

---

---

---

NADC-80135-60

A-7

NADC-80135-60

FIELD-1, FIELD-2, FIELD-3, FIELD-4, FIELD-5, FIELD-6, FIELD-7, FIELD-8, FIELD-9, FIELD-10

130-	PROF3	10	1	-45.
140-	PROF3	11	1	0.
141-	PROF3	12	1	-45.
142-	PROF3	13	1	45.
143-	PROF3	14	1	0.
144-	PROF3	15	1	0.
145-	PROF3	16	1	45.
146-	PROF3	17	1	-45.
147-	PROF3	18	1	0.
148-	PROF3	19	1	-45.
149-	PROF3	20	1	45.
150-	PROF3	21	1	0.
151-	PROF3	10	1	3
152-	PROF3	10	1	3
153-	PROF3	10	2	3
154-	PROF3	10	2	3
155-	PROF3	10	3	3
156-	PROF3	10	3	3
157-	PROF3	10	4	3
158-	PROF3	10	4	3
159-	PROF3	10	5	3
160-	PROF3	10	5	3
161-	PROF3	10	6	3
162-	PROF3	10	6	3
163-	PROF3	10	7	3
164-	PROF3	10	7	3
165-	PROF3	10	8	3
166-	PROF3	10	8	3
167-	PROF3	10	9	3
168-	PROF3	10	9	3
169-	PROF3	10	10	3
170-	PROF3	10	10	3
171-	PROF3	10	11	3
172-	PROF3	10	11	3
173-	PROF3	10	12	3
174-	PROF3	10	12	3
175-	PROF3	10	12	3
176-	PROF3	10	13	3
177-	PROF3	10	14	3
178-	PROF3	10	14	3
179-	PROF3	10	15	3
180-	PROF3	10	15	3
181-	PROF3	10	16	3
182-	PROF3	10	16	3
183-	PROF3	10	17	3
184-	PROF3	10	17	3

F U L K D A T A C A R D S

PAGE 5

CARD FIELD-1, FIELD-2, FIELD-3, FIELD-4, FIELD-5, FIELD-6, FIELD-7, FIELD-8, FIELD-9, FIELD-10

185-	SDC20	10	18	3	53	41	39	52	
186-	SDC20	10	18	3	53	42	40	52	
187-	SDC20	10	19	3	55	43	41	54	
188-	SDC20	10	19	3	55	44	42	54	
189-	SDC20	10	20	3	56	45	43	55	
190-	SDC20	10	20	3	56	46	44	55	
191-	SDC20	10	21	3	57	47	45	56	
192-	SDC20	10	21	3	57	48	46	56	
193-	SPC2	10	1	411	-.004243	0.	1	+S1	
194-	+S1	7							
195-	SPC2	10	1	421	-.003	0.			
196-	SPC2	10	1	431	-.003	0.			
197-	SPC2	10	1	441	-.004243	0.	1	+S2	
198-	+S2	7							
199-	SPC2	10	1	414	-.004243	0.	1	+S3	
200-	+S3	7							
201-	SPC2	10	1	424	-.003	0.			
202-	SPC2	10	1	434	-.003	0.			
203-	SPC2	10	1	444	-.004243	0.	1	+S4	
204-	+S4	7							
205-	SPC2	10	2	411	-.004243	0.	1	+S5	
206-	+S5	7							
207-	SPC2	10	2	421	-.003	0.			
208-	SPC2	10	2	431	-.003	0.			
209-	SPC2	10	2	441	-.004243	0.	1	+S6	
210-	+S6	7							
211-	SPC2	10	3	411	-.004243	0.	1	+S7	
212-	+S7	7							
213-	SPC2	10	3	421	-.003	0.			
214-	SPC2	10	3	431	-.003	0.			
215-	SPC2	10	3	441	-.004243	0.	1	+S8	
216-	+S8	7							
217-	SPC2	10	4	411	-.004243	0.	1	+S9	
218-	+S9	7							
219-	SPC2	10	4	421	-.003	0.			
220-	SPC2	10	4	431	-.003	0.			
221-	SPC2	10	4	441	-.004243	0.	1	+S10	
222-	+S10	7							
223-	SPC2	10	5	411	-.004243	0.	1	+S11	
224-	+S11	7							
225-	SPC2	10	5	421	-.003	0.			
226-	SPC2	10	5	431	-.003	0.			
227-	SPC2	10	5	441	-.004243	0.	1	+S12	
228-	+S12	7							
229-	SPC2	10	6	411	-.004243	0.	1	+S13	
230-	+S13	7							

NADC-80135-60

PAGE 6

P U L K   D A T A   C A R D S

CARD   FIELD-1, FIELD-2, FIELD-3, FIELD-4, FIELD-5, FIELD-6, FIELD-7, FIELD-8, FIELD-9, FIELD-10

231-	SPC2	10	6	421	-0.003	0.
232-	SPC2	10	6	431	-0.003	0.
233-	SPC2	10	6	441	-0.004243	0.
234-	+S14	7				+S14
235-	SPC2	10	7	411	-0.004243	0.
236-	+S15	7				+S15
237-	SPC2	10	7	421	-0.003	0.
238-	SPC2	10	7	431	-0.003	0.
239-	SPC2	10	7	441	-0.004243	0.
240-	+S16	7				+S16
241-	PARAM	ITER	1400			
242-	END DATA					

PATCHES-III INPUT DATA  
LAMINATE IMPACT  
STRUCTURAL RESPONSE MODEL

Case 1. (See Computer Listing)

Case 2. Change gridpoints 9, 11, 13, 14, 17, 19, 21, 23.

```
GRID, 9, , -0.356-2, -0.356-2
GRID, 11, , 0.356-2, -0.356-2
GRID, 13, , -0.178-2, -0.178-2
GRID, 15, , 0.178-2, -0.178-2
GRID, 17, , -0.178-2, 0.178-2
GRID, 19, , 0.178-2, 0.178-2
GRID, 21, , -0.356-2, 0.356-2
GRID, 23, , 0.356-2, 0.356-2
```

Case 3. Change gridpoints 5, 7, 29, 31 and redefine element number 11 data.

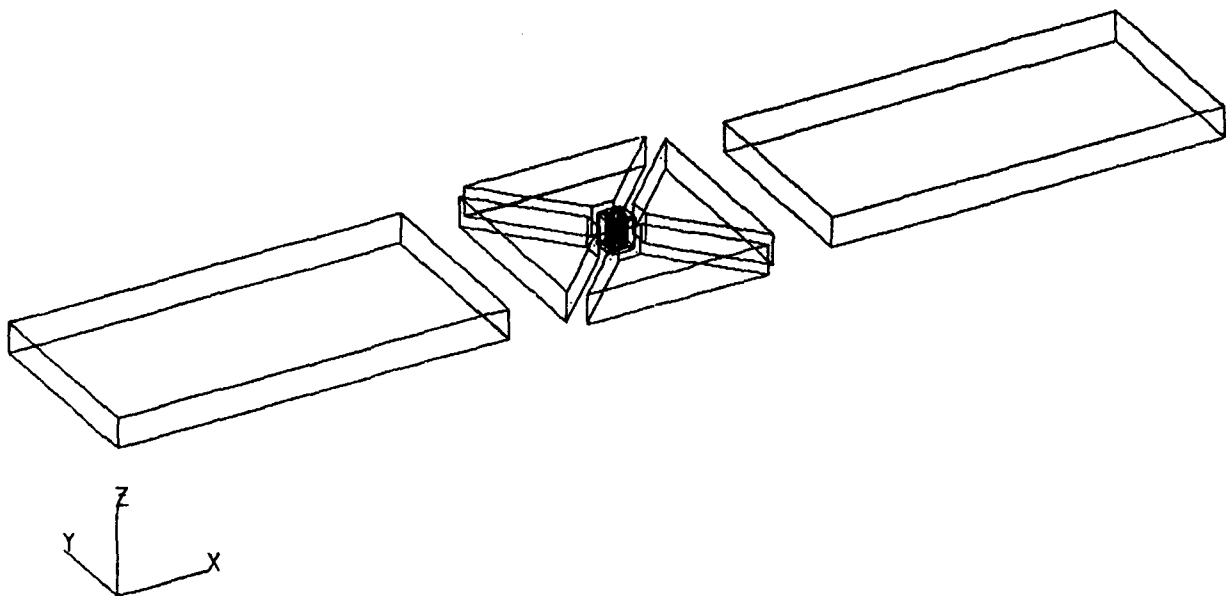
```
GRID, 5, , 10.16-2, -2.0-2
GRID, 7, , -10.16-2, -2.0-2
GRID, 29, , 10.16-2, 2.0-2
GRID, 31, , -10.16-2, 2.0-2
PATCHQ , 11, 7, 31, 25, 1
CPDE3 , 11, 7, 31, 25, 1
+C11 , CCL, 8, 32, 26, 2
SDC10 , 10, 11, 123, 7, 8, 32, 31
SDC10 , 10, 11, 2, 7, 1, 2, 8
SDC10 , 10, 11, 2, 31, 25, 26, 32
SDC10 , 10, 10, 123, 5, 6, 30, 29
```

(delete) SDC10 , 10, 8, 123, 1, 2, 26, 25

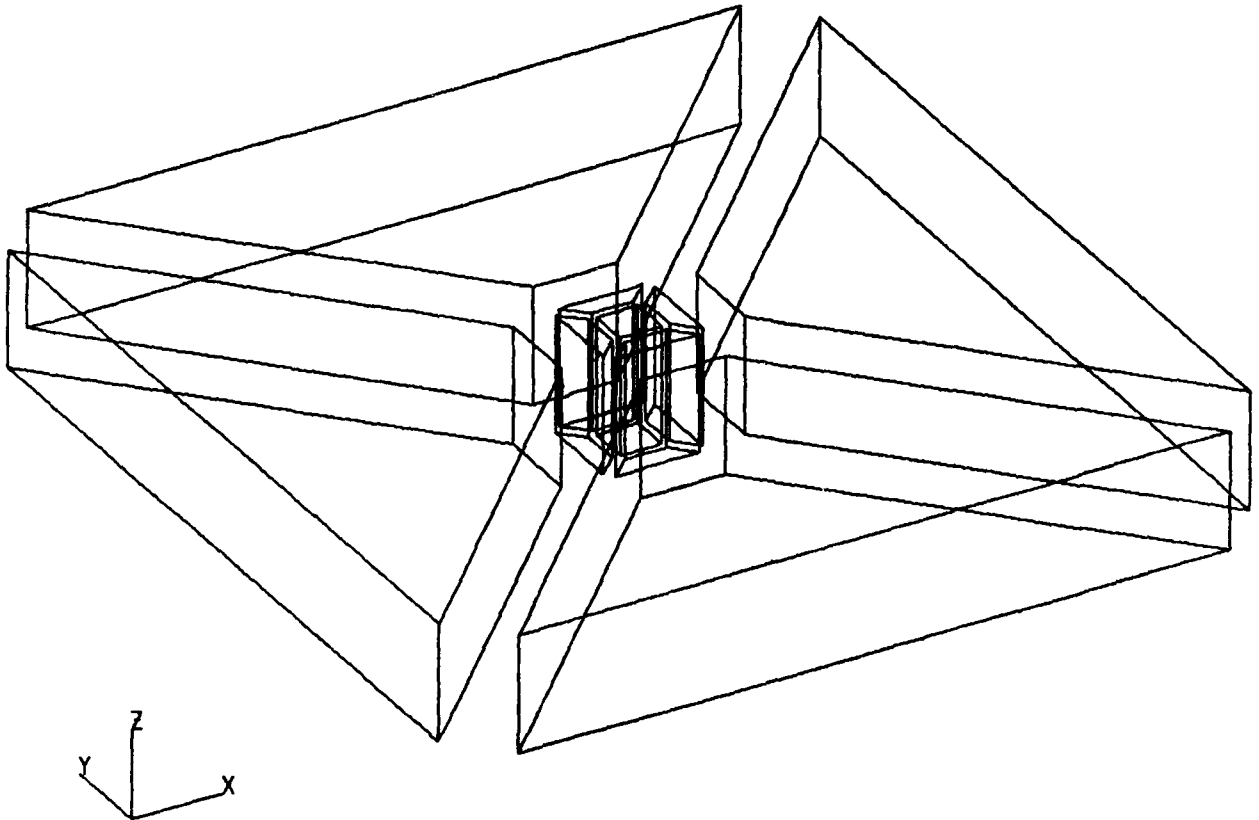
Case 4. Combine the changes for Cases 2 and 3.



LAMINATE STRUCTURAL RESPONSE MODEL  
FOR CASES 3 AND 4



IMPACT SITE STRUCTURAL RESPONSE MODEL  
FOR ALL CASES





22.45.06. 78/05/25.

CASE CONTROL DATA

TITLE = NADC LAMINATE IMPACT  
 SUBTITLE = 48 PLY MODEL \*\* VARIABLE PROPERTIES  
 SDC = 10  
 LOAD = 5  
 TIME = 17  
 CRPNT = FLEHENT.CG  
 OUTPUT  
 EVERYTHING  
 BEGIN RUN

PAGE 1

R U L K D A T A C A R D S

F1FD=1,F1FD=2,F1FD=3,F1FD=4,F1FD=5,F1FD=6,F1FD=7,F1FD=8,F1FD=9,F1FD=10

CARD

1-	CPDEF 1	13	17	19	15	+C1
2-	+C1	14	18	20	16	
3-	CPDEF 2	15	19	21	11	+C2
4-	+C2	16	20	34	12	
5-	CPDEF 3	17	21	23	19	+C3
6-	+C3	18	22	34	20	
7-	CPDEF 4	9	21	17	13	+C4
8-	+C4	10	22	18	14	
9-	CPDEF 5	9	13	15	11	+C5
10-	+C5	10	14	16	12	
11-	CPDEF 6	11	23	27	3	+C6
12-	+C6	12	34	28	4	
13-	CPDEF 7	21	25	27	23	+C7
14-	+C7	22	26	28	34	
15-	CPDEF 8	1	25	21	9	+C8
16-	+C8	2	26	22	10	
17-	CPDEF 9	1	9	11	3	+C9
18-	+C9	2	10	12	4	
19-	CPDEF 10	3	27	29	5	+C10
20-	+C10	4	28	30	6	
21-	CPDEF 11	5	29	31	7	+C11
22-	+C11	6	30	32	8	
23-	GRID 1		-1.905-2-2.0-2			
24-	GRID 3		1.905-2-2.0-2			
25-	GRID 5		8.255-2-2.0-2			
26-	GRID 7		18.415-2-2.0-2			
27-	GRID 9		-224-2			
28-	GRID 11		-224-2			
29-	GRID 13		-112-2			
30-	GRID 15		-112-2			
31-	GRID 17		-112-2			
32-	GRID 19		-112-2			
33-	GRID 21		-224-2			
34-	GRID 23		-224-2			
35-	GRID 25		-1.905-2 2.0-2			
36-	GRID 27		1.905-2 2.0-2			
37-	GRID 29		8.255-2 2.0-2			
38-	GRID 31		18.415-2 2.0-2			
39-	PATCHQ 1	13	17	19	15	
40-	PATCHQ 2	15	19	23	11	
41-	PATCHQ 3	17	21	23	19	
42-	PATCHQ 4	9	21	17	13	
43-	PATCHQ 5	9	13	15	11	
44-	PATCHQ 6	11	23	27	3	
45-	PATCHQ 7	21	25	27	23	
46-	PATCHQ 8	1	25	21	9	

**BULK DATA CARDS**

FIELD=1, FIELD=2, FIELD=3, FIELD=4, FIELD=5, FIELD=6, FIELD=7, FIELD=8, FIELD=9, FIELD=10

PATCHO	9	1	11	3	5	7
PATYCHO	10	27	29	5		
PATYCHO	11	29	31			
MPN	1	.6339A-2				
MPN	2	.6339A-2				
MPN	3	.6339A-2				
MPN	4	.6339A-2				
MPN	5	.6339A-2				
MPN	6	.6339A-2				
MPN	7	.6339A-2				
MPN	8	.6339A-2				
MPN	9	.6339A-2				
MPN	10	.6339A-2				
MPN	11	.6339A-2				
PPDE3	1					
PPDE3	2					
PPDE3	3					
PPDE3	4					
PPDE3	5					
PPDE3	6					
PPDE3	7					
PPDE3	8					
PPDE3	9					
PPDE3	10					
PPDE3	11					
MATC	1					
MTRX-1	72.622	24.173+92.379+9	9.432+9	22.091+90.	2.427+9+M2	
M2	0.	3.771+9 0.	3.744+9	2.427+90.		
MTRX-2	71.650+915.906+92.910+9	36.887+92.468+9	9.432+9	16.279+90.		
M3	0.	3.771+9 0.	3.744+9	2.427+90.		
M4	1	1	1	1	1	1
M5	1	1	1	1	1	1
M6	2	2	2	2	2	2
M7	2	2	2	2	2	2
M8	2	2	2	2	2	2
M9	1	1	1	1	1	1
M10	1	1	1	1	1	1
M11	9	9	9	9	9	9
M12	10	10	10	10	10	10
M13	10	10	10	10	10	10
M14	10	10	10	10	10	10
M15	10	10	10	10	10	10
M16	10	10	10	10	10	10
M17	10	10	10	10	10	10
M18	10	10	10	10	10	10
M19	10	10	10	10	10	10
M20	10	10	10	10	10	10
M21	10	10	10	10	10	10
M22	10	10	10	10	10	10
M23	10	10	10	10	10	10
M24	10	10	10	10	10	10
M25	10	10	10	10	10	10
M26	10	10	10	10	10	10
M27	10	10	10	10	10	10
M28	10	10	10	10	10	10
M29	10	10	10	10	10	10
M30	10	10	10	10	10	10
M31	10	10	10	10	10	10
M32	10	10	10	10	10	10
M33	10	10	10	10	10	10
M34	10	10	10	10	10	10
M35	10	10	10	10	10	10
M36	10	10	10	10	10	10
M37	10	10	10	10	10	10
M38	10	10	10	10	10	10
M39	10	10	10	10	10	10
M40	10	10	10	10	10	10
M41	10	10	10	10	10	10
M42	10	10	10	10	10	10
M43	10	10	10	10	10	10
M44	10	10	10	10	10	10
M45	10	10	10	10	10	10
M46	10	10	10	10	10	10
M47	10	10	10	10	10	10
M48	10	10	10	10	10	10
M49	10	10	10	10	10	10
M50	10	10	10	10	10	10
M51	10	10	10	10	10	10
M52	10	10	10	10	10	10
M53	10	10	10	10	10	10
M54	10	10	10	10	10	10
M55	10	10	10	10	10	10
M56	10	10	10	10	10	10
M57	10	10	10	10	10	10
M58	10	10	10	10	10	10
M59	10	10	10	10	10	10
M60	10	10	10	10	10	10
M61	10	10	10	10	10	10
M62	10	10	10	10	10	10
M63	10	10	10	10	10	10
M64	10	10	10	10	10	10
M65	10	10	10	10	10	10
M66	10	10	10	10	10	10
M67	10	10	10	10	10	10
M68	10	10	10	10	10	10
M69	10	10	10	10	10	10
M70	10	10	10	10	10	10
M71	10	10	10	10	10	10
M72	10	10	10	10	10	10
M73	10	10	10	10	10	10
M74	10	10	10	10	10	10
M75	10	10	10	10	10	10
M76	10	10	10	10	10	10
M77	10	10	10	10	10	10
M78	10	10	10	10	10	10
M79	10	10	10	10	10	10
M80	10	10	10	10	10	10
M81	10	10	10	10	10	10
M82	10	10	10	10	10	10
M83	10	10	10	10	10	10
M84	10	10	10	10	10	10
M85	10	10	10	10	10	10
M86	10	10	10	10	10	10
M87	10	10	10	10	10	10
M88	10	10	10	10	10	10
M89	10	10	10	10	10	10
M90	10	10	10	10	10	10
M91	10	10	10	10	10	10
M92	10	10	10	10	10	10
M93	10	10	10	10	10	10
M94	10	10	10	10	10	10
M95	10	10	10	10	10	10
M96	10	10	10	10	10	10
M97	10	10	10	10	10	10
M98	10	10	10	10	10	10
M99	10	10	10	10	10	10
M100	10	10	10	10	10	10

PAGE 3

BULK DATA CARDS

FIELD-1, FIELD-2, FIELD-3, FIELD-4, FIELD-5, FIELD-6, FIELD-7, FIELD-8, FIELD-9, FIELD-10

CARD

93-  
94-  
95-  
96-  
97-  
98-  
99-  
100-  
101-

SDC10 10 7 2 25 27 28 26 25  
SDC10 10 8 123 1 2 26 25  
HPATCH 1 P 20 14 18 20 16  
MTRX=20 0. 0. 0. 0. 1. 1.  
+01 0. 1. 1. 0. 0. 0.  
PIAD3 5 1 -1.576+9  
PARAM ITER 700  
PARAM DERIG 1  
END DATA

+D1  
0.  
0.

PATCHES-III INPUT DATA

LAMINATE IMPACT

IMPACT SITE MODEL

- Case 1. (See Computer Listing)
- Case 2. (See Computer Listing Page A-29 for gridpoint changes).
- Case 3. Same as Case 1 with new structural response input data.
- Case 4. Same as Case 2 with new structural response input data.





## CASE CONTROL DATA

16.35.07. 78/11709.25

TITLE = INTERPLANAR STRESS GRADIENT ANALYSIS MODEL  
 SUBTITLE = 48 PLY LAMINATE

SDC = 10

LOAD = 16

TIME = 30

RSTART = CG

OUTPUT

SET 1 = ALL

VOLUME = 1

FOTSP = 1

ESTRAIN = 1

FSTRESS = 1

ELOAD = 1

EPODCE = 1

MSTRESS = 1

MSTRAIN = 1

BEGIN BULK

QUICK DATA CARDS

FIELD-1, FIELD-2, FIELD-3, FIELD-4, FIELD-5, FIELD-6, FIELD-7, FIELD-8, FIELD-9, FIELD-10

CARD

1-	CPDE3	21	2	2	22	A2	+C1
2-	+C1		1	1	21	81	
3-	CPDE3	41	2	2	42	22	+C2
4-	+C2		1	1	41	21	
5-	CPDE3	61	2	2	62	42	+C3
6-	+C3		1	1	61	41	
7-	CPDE3	81	2	2	82	62	+C4
8-	+C4		1	1	81	61	
9-	CPDE3	121	A2	22	122	1A2	+C5
10-	+C5		A1	21	121	1A1	
11-	CPDE3	141	22	42	142	122	+C6
12-	+C6		21	41	141	121	
13-	CPDE3	161	42	62	162	142	+C7
14-	+C7		41	61	161	141	
15-	CPDE3	181	62	A2	182	162	+C8
16-	+C8		61	A1	181	161	
17-	CPDE3	22	3	3	23	A3	+C9
18-	+C9		2	3	22	A2	
19-	CPDE3	42	3	3	43	23	+C10
20-	+C10		2	2	42	23	
21-	CPDE3	62	3	3	63	43	+C11
22-	+C11		2	2	62	42	
23-	CPDE3	A2	3	3	A3	63	+C12
24-	+C12		2	2	A2	62	
25-	CPDE3	122	83	23	123	1P3	+C13
26-	+C13		A2	22	122	1P2	
27-	CPDE3	142	23	43	143	123	+C14
28-	+C14		22	42	142	122	
29-	CPDE3	162	43	63	163	143	+C15
30-	+C15		42	62	162	142	
31-	CPDE3	182	63	A3	183	163	+C16
32-	+C16		62	A2	182	162	
33-	CPDE3	23	4	4	24	84	+C17
34-	+C17		3	3	23	A3	
35-	CPDE3	43	4	4	44	24	+C18
36-	+C18		3	3	43	23	
37-	CPDE3	63	4	4	64	44	+C19
38-	+C19		3	3	63	43	
39-	CPDE3	A3	4	4	A4	64	+C20
40-	+C20		3	3	A3	63	
41-	CPDE3	123	A4	24	124	184	+C21
42-	+C21		A3	23	123	183	
43-	CPDE3	143	24	44	144	124	+C22
44-	+C22		23	43	143	123	
45-	CPDE3	163	44	64	164	144	+C23
46-	+C23		43	63	163	143	

PAGE 2

RULK DATA CARDS

FIELD=1, FIELD=2, FIELD=3, FIELD=4, FIELD=5, FIELD=6, FIELD=7, FIELD=8, FIELD=9, FIELD=10

47-	CPNE3	183	64	84	184	164	+C24
48-	+C24		63	83	183	163	
49-	CPNE3	24	5	5	25	85	+C25
50-	+C25		4	4	24	84	
51-	CPNE3	44	5	5	45	25	+C26
52-	+C26		4	4	44	24	
53-	CPNE3	64	5	5	65	45	+C27
54-	+C27		4	4	64	44	
55-	CPNE3	84	5	5	85	65	+C28
56-	+C28		4	4	84	64	
57-	CPNE3	124	85	25	125	185	+C29
58-	+C29		84	24	124	184	
59-	CPNE3	144	25	45	145	125	+C30
60-	+C30		24	44	144	124	
61-	CPNE3	164	45	65	165	145	+C31
62-	+C31		44	64	164	144	
63-	CPNE3	184	65	85	185	165	+C32
64-	+C32		64	84	184	164	
65-	GRID	1		0	0	63398-2	
66-	GRID	2		0	0	62078-2	
67-	GRID	3		0	0	60758-2	
68-	GRID	4		0	0	58115-2	
69-	GRID	5		0	0	58115-2	
70-	GRID	81		7920-3	7920-3	63398-2	
71-	GRID	82		7920-3	7920-3	62078-2	
72-	GRID	83		7920-3	7920-3	60758-2	
73-	GRID	84		7920-3	7920-3	58115-2	
74-	GRID	85		7920-3	7920-3	58115-2	
75-	GRID	121		2240-2	2240-2	63398-2	
76-	GRID	122		2240-2	2240-2	62078-2	
77-	GRID	123		2240-2	2240-2	60758-2	
78-	GRID	124		2240-2	2240-2	58115-2	
79-	GRID	125		2240-2	2240-2	58115-2	
80-	GRID	141		2240-2	2240-2	63398-2	
81-	GRID	142		2240-2	2240-2	62078-2	
82-	GRID	143		2240-2	2240-2	60758-2	
83-	GRID	144		2240-2	2240-2	58115-2	
84-	GRID	145		2240-2	2240-2	58115-2	
85-	GRID	161		2240-2	2240-2	63398-2	
86-	GRID	162		2240-2	2240-2	62078-2	
87-	GRID	163		2240-2	2240-2	60758-2	
88-	GRID	164		2240-2	2240-2	58115-2	
89-	GRID	165		2240-2	2240-2	58115-2	
90-	GRID	181		2240-2	2240-2	63398-2	
91-	GRID	182		2240-2	2240-2	62078-2	
92-	GRID	183		2240-2	2240-2	60758-2	

**PUBLIC DATA CARDS**

2240-2-2240-2, 58115-2  
2240-2-2240-2, 0

93-	GRTO	184
94-	GRTO	184
95-	LINEPC	1
96-	LINEPC	2
97-	LINEPC	3
98-	LINEPC	4
99-	PATCHM	21
100-	PATCHR	22
101-	PATCHR	23
102-	PATCHR	24
103-	PATCHR	41
104-	PATCHR	42
105-	PATCHR	43
106-	PATCHR	44
107-	PATCHR	61
108-	PATCHR	62
109-	PATCHR	63
110-	PATCHR	64
111-	PATCHR	81
112-	PATCHR	82
113-	PATCHR	93
114-	PATCHR	94
115-	PATCHQ	121
116-	PATCHQ	122
117-	PATCHQ	123
118-	PATCHQ	124
119-	PATCHQ	141
120-	PATCHQ	142
121-	PATCHQ	143
122-	PATCHQ	144
123-	PATCHQ	161
124-	PATCHQ	162
125-	PATCHQ	163
126-	PATCHQ	164
127-	PATCHQ	181
128-	PATCHQ	182
129-	PATCHQ	183
130-	PATCHQ	184
131-	PATCHQ	101
132-	PATCHQ	102
133-	PATCHQ	103
134-	PATCHQ	104
135-	HP2PAT	121
136-	HP2PAT	141
137-	HP2PAT	161
138-	HP2PAT	181

0.	90.
0.	90.
0.	90.
0.	90.
90.	180.
90.	180.
90.	180.
90.	180.
180.	270.
180.	270.
140.	270.
270.	360.
270.	360.
270.	360.

122	121	181
123	122	182
124	123	183
125	124	184
142	141	121
143	142	122
144	143	123
145	144	124
162	161	141
163	162	142
164	163	143
165	164	144
182	181	161
183	182	162
184	183	163
185	184	164
22	81	1
23	82	2
24	83	3
25	84	4
21		
41		
61		
81		

PATCHQ	121	182
PATCHQ	122	183
PATCHQ	123	184
PATCHQ	124	185
PATCHQ	141	122
PATCHQ	142	123
PATCHQ	143	124
PATCHQ	144	125
PATCHQ	161	142
PATCHQ	162	143
PATCHQ	163	144
PATCHQ	164	145
PATCHQ	181	162
PATCHQ	182	163
PATCHQ	183	164
PATCHQ	184	165
PATCHQ	101	2
PATCHQ	102	3
PATCHQ	103	4
PATCHQ	104	5
HP2PAT	121	121
HP2PAT	141	141
HP2PAT	161	161
HP2PAT	181	181

## FIELD=1, FIELD=2, FIELD=3, FIELD=4, FIELD=5, FIELD=6, FIELD=7, FIELD=8, FIELD=9, FIELD=10

139-	WP2PAT	122	122	22
140-	WP2PAT	142	142	42
141-	WP2PAT	162	162	62
142-	WP2PAT	182	182	82
143-	WP2PAT	123	123	23
144-	WP2PAT	143	143	43
145-	WP2PAT	163	163	63
146-	WP2PAT	183	183	83
147-	WP2PAT	124	124	24
148-	WP2PAT	144	144	44
149-	WP2PAT	164	164	64
150-	WP2PAT	184	184	84
151-	WPR	21	101	
152-	WPR	41	101	
153-	WPR	61	101	
154-	WPR	81	101	
155-	WPR	22	102	
156-	WPR	42	102	
157-	WPR	62	102	
158-	WPR	82	102	
159-	WPR	23	103	
160-	WPR	43	103	
161-	WPR	63	103	
162-	WPR	83	103	
163-	WPR	24	104	
164-	WPR	44	104	
165-	WPR	64	104	
166-	WPR	84	104	
167-	SOC1	10	121	21
168-	SOC1	10	122	22
169-	SOC1	10	123	23
170-	SOC1	10	124	24
171-	SOC1	10	141	41
172-	SOC1	10	142	42
173-	SOC1	10	143	43
174-	SOC1	10	144	44
175-	SOC1	10	161	61
176-	SOC1	10	162	62
177-	SOC1	10	163	63
178-	SOC1	10	164	64
179-	SOC1	10	181	81
180-	SOC1	10	182	82
181-	SOC1	10	183	83
182-	SOC1	10	184	84
183-	PPDE3	21	2	
184-	PPDE3	41	2	

[illegible]

21	121	221
22	122	222
23	123	223
24	124	224
41	141	241
42	142	242
43	143	243
44	144	244
61	161	261
62	162	262
63	163	263
64	164	264
81	181	281
82	182	282
83	183	283
84	184	284
	45.0	
	45.0	

# RAUL K DATA CARDS

CARD FIELD=1, FIELD=2, FIELD=3, FIELD=4, FIELD=5, FIELD=6, FIELD=7, FIELD=8, FIELD=9, FIELD=10

[illegible]

BU LK 350 ATT A C A R D S

FIELD=1,FIELD=2,FIELD=3,FIELD=4,FIFD=5,FIFD=6,FIELD=7,FIELD=8,FIELD=9,FIELD=10

**CARD**

[illegible]



PAGE 7

R I I K DATA CARDS

FIELD=1, FIELD=2, FIELD=3, FIELD=4, FIELD=5, FIELD=6, FIELD=7, FIELD=8, FIELD=9, FIELD=10

CARD

279-	DPATQ	182	2	163	162	182	183			
280-	DPATQ	282	3	163	162	182	183			
281-	DPATQ	43	1	164	163	183	184			
282-	DPATQ	183	2	164	163	183	184			
283-	DPATQ	243	3	164	163	183	184			
284-	DPATQ	44	1	165	164	184	185			
285-	DPATQ	144	2	165	164	184	185			
286-	DPATQ	284	3	165	164	184	185			
287-	DPATCH	1	P	10	1	1	21	R1		
288-	DPATCH	2	P	10	1	1	41	21		
289-	DPATCH	3	P	10	1	1	61	41		
290-	DPATCH	4	P	10	1	1	81	61		
291-	MTX-10	1.0		.942809	.745356	0.	1.0			
292-	+MX10	1.0		.942809	.745356	0.	1.0			
293-	PLNAD3	16	21	1	-1.814+9					
294-	PLNAD3	16	41	2	-1.814+9					
295-	PLNAD3	16	61	3	-1.814+9					
296-	PLNAD3	16	R1	4	-1.814+9					
297-	END DATA									

+MX10

NADC801LOG11  
NADC DATA

22-MAR-1980 12:03:03.44

PAGE 4

22-MAR-80

12:02:30

PAGE 2

P A T C H E S   D A T A   D I R E C T I V E S

1.	GRID 1	0.0	0.0	.63308-2
2.	GRID 2	0.0	0.0	.62078-2
3.	GRID 3	0.0	0.0	.60758-2
4.	GRID 4	0.0	0.0	.58115-2
5.	GRID 5	0.0	0.0	.0
6.	GRID A1	.1259-2	.1259-2	.63398-2
7.	GRID A2	.1259-2	.1259-2	.62078-2
8.	GRID A3	.1259-2	.1259-2	.60758-2
9.	GRID A4	.1259-2	.1259-2	.58115-2
10.	GRID A5	.1259-2	.1259-2	.0
11.	GRID 121	.3560-2	.3560-2	.63398-2
12.	GRID 122	.3560-2	.3560-2	.62078-2
13.	GRID 123	.3560-2	.3560-2	.60758-2
14.	GRID 124	.3560-2	.3560-2	.58115-2
15.	GRID 125	.3560-2	.3560-2	.0
16.	GRID 141	.3560-2	.3560-2	.63398-2
17.	GRID 142	.3560-2	.3560-2	.62078-2
18.	GRID 143	.3560-2	.3560-2	.60758-2
19.	GRID 144	.3560-2	.3560-2	.58115-2
20.	GRID 145	.3560-2	.3560-2	.0
21.	GRID 161	.3560-2	.3560-2	.63398-2
22.	GRID 162	.3560-2	.3560-2	.62078-2
23.	GRID 163	.3560-2	.3560-2	.60758-2
24.	GRID 164	.3560-2	.3560-2	.58115-2
25.	GRID 165	.3560-2	.3560-2	.0
26.	GRID 181	.3560-2	.3560-2	.63398-2
27.	GRID 182	.3560-2	.3560-2	.62078-2
28.	GRID 183	.3560-2	.3560-2	.60758-2
29.	GRID 184	.3560-2	.3560-2	.58115-2
30.	GRID 185	.3560-2	.3560-2	.0
31.	END DATA			

PATCHES-III SCHEMATIC  
LAMINATE IMPACT  
IMPACT SITE 12 PLY MODEL

The input data for this model are a direct extension of the 4 ply model with 32 finite elements increased to 88 finite elements. If the findings of the present report are used, then one plane of symmetry ( $e_1, e_3$ ) can be used to reduce the number of elements. In this instance the topologically equivalent model would have 66 finite elements. To reduce this number further will require a change to the basic layout used in this report.



## D I S T R I B U T I O N L I S T

## Government Activities

	<u>No. of Copies</u>
NAVAIRSYSCOM, (AIR-950D), 2 for retention, 2 for AIR-530, 1 for AIR-320B, AIR-52032D, AIR-5302, AIR-53021, AIR-530215). . . . .	9
AFFDL, WPAFB, OH 45433	
(Attn: FBE) . . . . .	1
(Attn: FBS/Mr. L. Kelly). . . . .	1
(Attn: FBS/Mr. C. Wallace). . . . .	1
(Attn: FBC/Mr. J. Wood) . . . . .	1
(Attn: AFML/MBM Dr. S. Tsai). . . . .	1
(Attn: AFML/LTN Mr. R. L. Rapson) . . . . .	1
(Attn: MBC/Reinhart). . . . .	1
(Attn: MXA/Feccheck) . . . . .	1
AFOSR, Washington, D.C. 20333	
(Attn: Dr. W. Walker) . . . . .	1
DTIC . . . . .	12
FAA, Washington, D.C. 20553	
(Attn: R. Allen-AWS/120). . . . .	1
NAEC, Lakehurst, NJ 08753	
(Attn: Mr. D. W. Nesterok/Code 92713) . . . . .	1
NASA (ADM), Washington, D.C. 20546	
(Attn: Secretary) . . . . .	1
NASA, George C. Marshall Space Flight Center, Huntsville, AL 35812	
(Attn: S&E-ASTN-ES/Mr. E. E. Engler). . . . .	1
(Attn: S&E-ASTN-M/Mr. R. Schwinghamer). . . . .	1
(Attn: S&E-ASTM-MNM/Dr. J. M. Stuckey . . . . .	1
NASA, Langley Research Center, Hampton, VA 23365	
(Attn: Mr. J. P. Peterson, Mr. R. Pride, and Dr. M. Card) . .	3
NASA, Lewis Research Center, Cleveland, OH 44153	
(Attn: Technical Library, and M. Hershberg) . . . . .	2
NAVPGSCHL, Monterey, CA 95940	
(Attn: Prof. R. Ball, Prof. M. H. Bank) . . . . .	2
NAVSEASYSYSCOM, Washington, D.C. 20362	
(Attn: Code 035, Mr. C. Pohler) . . . . .	1
NAVSEC, Arlington, VA 20360	
(Attn: NSEC-6101E). . . . .	1
NAVSHIPRANDCEN, Bethesda, MD 20034	
(Attn: Code 173.2, Mr. W. P. Cauch) . . . . .	1
NAVSHIPRANDCEN, Annapolis, MD 21402	
(Attn: Code 2870, Mr. H. Edelstein) . . . . .	1
NOL, White Oak, MD 20910	
(Attn: Mr. F. R. Barnet). . . . .	1
NRL, Washington, D.C. 20375	
(Attn: Dr. I. Wolock) . . . . .	1

## Government Activities (Continued)

	<u>No. of Copies</u>
NAVAIRDEVCON, Warminster, PA 18974 (Attn: Major J. C. Lillie - 097). . . . .	1
CNR Washington, D.C. 20362 (Attn: Dr. N. Perrone). . . . .	1
PLASTEC, Picatinny Arsenal, Dover, NJ 07801 (Attn: Librarian, Bldg. 176, SARPA-FR-M-D and Mr. H. Pebly) . .	2
USAAVMATLAB, Fort Eustis, VA 23603 (Attn: Mr. A. Gustafson). . . . .	1
USAMATRESAG, Watertown, MA (Attn: Dr. E. Lenoe). . . . .	1
USARESOFC, Durham, NC 27701. . . . .	1

## Non-Government Agencies

Avco Aero Structures Division, Nashville, TN 37202 (Attn: Mr. W. Ottenville). . . . .	1
Batelle Columbus Laboratories, Metals and Ceramics Information Center, 505 King Avenue, OH 43201. . . . .	1
Bell Aerospace Company, Buffalo, NY 14240 (Attn: Zone I-85, Mr. F. M. Anthony). . . . .	1
Bell Helicopter Company, Fort Worth, TX 76100 (Attn: Mr. Charles Harvey). . . . .	1
Bendix Products Aerospace Division, South Bend, IN 46619 (Attn: Mr. R. V. Cervelli). . . . .	1
Boeing Aerospace Company, P.O. Box 3999, Seattle, WA 98124 (Attn: Code 206, Mr. R. E. Horton). . . . .	1
Boeing Company, Renton, Washington 98055 (Attn: Dr. R. June). . . . .	1
Boeing Company, Vertol Division, Philadelphia, PA 19142 (Attn: Mr. R. L. Pinckney, Mr. D. Hoffstedt). . . . .	2
Boeing Company, Wichita, KS 67210 (Attn: V. Reneau/MS 16-39). . . . .	1
Cabot Corp., Billerica Research Center, Billerica, MA 01821. . . .	1
Drexel University, Philadelphia, PA 19104 (Attn: Dr. P. C. Chou). . . . .	1
(Attn: Dr. A. S. D. Wang). . . . .	1
Effects Technology, Inc., 5383 Hollister Avenue, P.O. Box 30400, Santa Barbara, CA 93105 (Attn: Robert Globus). . . . .	1
E. I. DuPont Company, Wilmington, DE 19898 (Attn: Dr. J. Pigoiacampi). . . . .	1
Fairchild Industries, Hagerstown, MD 21740 (Attn: Mr. D. Buck). . . . .	1
Georgia Institute of Technology, Atlanta, GA (Attn: Prof. W. H. Horton). . . . .	1
General Dynamics/Convair, San Diego, CA 92138 (Attn: Mr. D. R. Dunbar, W. G. Scheck). . . . .	2
General Dynamics, Fort Worth, TX 76101 (Attn: Mr. J. A. Fant (Mail Zone-2844)) . . . . .	1
(Attn: Mr. D. Wilkins (Composite Structures Eng. Dept.)). . . .	1

## Non-Government Agencies (Continued)

	<u>No. of Copies</u>
General Electric Company, Philadelphia, PA 19101 (Attn: Mr. L. McCreight) . . . . .	1
Great Lakes Carbon Corporation, New York, NY 10017 (Attn: Mr. W. R. Benn, Mgr., Market Development) . . . . .	1
School of Engineering & Applied Science, Materials Research Laboratory, Washington University, Campus Box 1087, St. Louis, MO 63130 (Attn: T. Hahn) . . . . .	1
University of Delaware, Mechanics & Aerospace Eng. Dept., Evans Hall, Newark, DE 19711 (Attn: Dr. R. B. Pipes) . . . . .	1
Grumman Aerospace Corporation, Bethpage, L.I., NY 11714 (Attn: Mr. R. Hadcock, Mr. S. Dastin) . . . . .	2
Hercules Powder Company, Inc., Cumberland, MD 21501 (Attn: Mr. D. Hug) . . . . .	1
H. I. Thompson Fiber Glass Company, Gardena, CA 90249 (Attn: Mr. N. Myers) . . . . .	1
ITT Research Institute, Chicago, IL 60616 (Attn: Mr. K. Hofar) . . . . .	1
J. P. Stevens & Co., Inc., New York, NY 10036 (Attn: Mr. H. I. Shulock) . . . . .	1
Kaman Aircraft Corporation, Bloomfield, CT 06002 (Attn: Tech. Library) . . . . .	1
Lehigh University, Bethlehem, PA 18015 (Attn: Dr. G. C. Sih) . . . . .	1
Lockheed-California Company, Burbank, CA 91520 (Attn: Mr. E. K. Walker, Mr. Vaughn) . . . . .	2
Lockheed-Georgia Company, Marietta, GA 30063 (Attn: Technical Information Dept., Dept. 72-34, Zone 26) . . . . .	1
Vought Corporation, Dallas, TX 75222 (Attn: Mr. O. E. Dhonau/2-53442, C. R. Foreman) . . . . .	2
Martin Company, Baltimore, MD 21203 (Attn: Mr. J. E. Pawken) . . . . .	1
Materials Sciences Corp., Blue Bell, PA 19422 . . . . .	1
McDonnell Douglas Corporation, St. Louis, MO 63166 (Attn: Mr. Harold Dill, C. Stenberg, R. Garret) . . . . .	3
McDonnell Douglas Corporation, Long Beach, CA 90801 (Attn: H. C. Schjulderup, G. Lehman) . . . . .	2
Minnesota Mining & Manufacturing Company, St. Paul, MN 55104 (Attn: Mr. W. Davis) . . . . .	1
Northrop Aircraft Corp., Norair Division, Hawthorne, CA 90250 (Attn: Mr. R. D. Hayes, Mr. D. Stansbarger, Mr. R. C. Isemann, Mr. R. M. Veritte) . . . . .	4
Rockwell International, Columbus, OH 43216 (Attn: Mr. F. Kaufman) . . . . .	2
Rockwell International, Los Angeles, CA 90053 (Attn: Dr. L. Lackman) . . . . .	1
Rockwell International, Tulsa, OK 74151 (Attn: Mr. E. Sanders, Mr. J. H. Powell) . . . . .	2

## Non-Government Agencies (Continued)

	<u>No. of Copies</u>
Ownes Corning Fiberlass, Granville, OH 43023 (Attn: Mr. D. Mettes) . . . . .	1
Rohr Corporation, Riverside, CA 92503 (Attn: Dr. F. Riel and Mr. R. Elkin) . . . . .	2
Ryan Aeronautical Company, San Diego, CA 92112 (Attn: Mr. R. Long) . . . . .	1
Sikorsky Aircraft, Stratford, CT 06497 (Attn: Mr. J. Ray) . . . . .	1
University of Oklahoma, Norman, OK 93069 (Attn: Dr. G. M. Nordby) . . . . .	1
Union Carbide Corporation, Cleveland, OH 44101 (Attn: Dr. H. F. Volk) . . . . .	1
University of Wyoming, Laramie, WY 82071 (Attn: Dr. D. F. Adams) . . . . .	1
Virginia Tech, Blacksburg, VA 24061 (Attn: Dr. K. Reifsnider) . . . . .	1
Composittek Engineering Corp., 6925-1 Aragon Circle, Buena Park, CA 90620 (Attn: Mr. J. V. Noyes) . . . . .	1
Lockheed-California Co., Rye Canyon Research Lab, Burbank CA 91520 (Attn: Mr. Don E. Pettit) . . . . .	1
Villanova University, Philadelphia, PA 19085 (Attn: Dr. P. V. McLaughlin) . . . . .	1